# In Situ Surface-Directed Assembly of 2D Metal Nanoplatelets for Drug-Free Treatment of Antibiotic-Resistant Bacteria

*Parinaz Fathi, Ayman Roslend, Maha Alafeef, Parikshit Moitra, Ketan Dighe, Mandy B. Esch, and Dipanjan Pan**

**The development of antibiotic resistance among bacterial strains is a major global public health concern. To address this, drug-free antibacterial approaches are needed. Copper surfaces have long been known for their antibacterial properties. In this work, a one-step surface modification technique is used to assemble 2D copper chloride nanoplatelets directly onto copper surfaces such as copper tape, transmission electron microscopy (TEM) grids, electrodes, and granules. The nanoplatelets are formed using copper ions from the copper surfaces, enabling their direct assembly onto these surfaces in a one-step process that does not require separate nanoparticle synthesis. The synthesis of the nanoplatelets is confirmed with TEM, scanning electron microscopy, energy dispersive spectroscopy (EDS), X-ray diffraction (XRD), and Fourier transform infrared spectroscopy (FT-IR). Antibacterial properties of the Cu nanoplatelets are demonstrated in multidrug-resistant (MDR) *Escherichia coli*, MDR *Acinetobacter baumannii*, MDR *Staphylococcus aureus*, *E. coli*, and *Streptococcus mutans*. Nanoplatelets lead to a marked improvement in antibacterial properties compared to the copper surfaces alone, affecting bacterial cell morphology, preventing bacterial cell division, reducing their viability, damaging bacterial DNA, and altering protein expression. This work presents a robust method to directly assemble copper nanoplatelets onto any copper surface to imbue it with improved antibacterial properties.**

## 1. Introduction

Drug-resistant bacterial infections are a ris-ing concern with increasing prescription of antibiotics. High-touch surfaces have been proven to contribute to pathogen spread.[1] Bacterial biofilms are typically the main form of surface bacterial contamination and are known to exhibit enhanced resistance to antibiotics.[2,3] This enhanced tolerance has been attributed to the stratified metabolic activity of the resident bacteria within the ultrastructure of the biofilm, increased mu-tation frequency of biofilm bacteria, and ability for inter-bacterial transfer of plas-mids that encodes for resistance toward an-timicrobial agents, among other factors.[3–5] Because of this, biofilm-infected surfaces pose a significant threat to public health—biofilm which originates from medical im-plants such as catheters, heart valves, and orthopedic implants can cause bloodstream and urinary tract infections.[4,6]

To address the potential health threat of biofilm-infected surfaces, many approaches have been explored to confer antibacte-rial properties to surfaces. In preventing

P. Fathi, A. Roslend, M. Alafeef, K. Dighe, D. Pan
Departments of Bioengineering, Materials Science and Engineering and Beckman Institute
University of Illinois at Urbana-Champaign
Urbana, IL 61801, USA
E-mail: dipanjan@psu.edu

M. Alafeef, P. Moitra, K. Dighe, D. Pan
Departments of Diagnostic Radiology Nuclear Medicine and Pediatrics University of Maryland School of Medicine
Baltimore, MD 21201, USA

M. Alafeef, K. Dighe, D. Pan
Department of Chemical and Biochemical Engineering University of Maryland Baltimore County
Baltimore, MD 21250, USA

M. Alafeef, P. Moitra, D. Pan
Department of Nuclear Engineering and Materials Science and Engineering Huck Institutes for the Life Sciences
The Pennsylvania State University
University Park, PA 16802, USA

M. B. Esch
Biomedical Technologies Group
Microsystems and Nanotechnology Division
Physical Measurement Laboratory
National Institute of Standards and Technology Gaithersburg, MD 20899, USA

M. Alafeef
Biomedical Engineering Department
Jordan University of Science and Technology
Irbid 22110, Jordan

bacterial growth, surfaces are typically modified via fabrication methods or treated with bactericidal agents to either prevent initial bacterial attachment onto the surface or kill the bacterial cells upon coming into contact with the surface, thereby preventing biofilm formation altogether.[7] Nanomaterials have been successfully synthesized for use in a variety of applications in medicine,[8–19] including the detection and eradication of bacteria.[20–38] Due to the proficient bactericidal abilities exhibited by metallic nanoparticles, particularly those composed of transition metals such as silver, copper, and gold, many have explored the utility of these particles for developing antibacterial surfaces.[7,39–43] These particles are typically synthesized and then integrated into polymer-based coatings for the controlled release of metal ions onto the local environment of the surface, killing bacterial cells upon making contact to the surface and therefore preventing biofilm formation.[44–47] Another approach involves fabricating surfaces with nano- or microstructures to improve their bacterial repellent properties.[48] This method employs laser ablation to form crater-like structures on the surface to minimize contact points between bacterial cells and the fabricated surface, subsequently conferring superhydrophobicity to the surface which helps prevent bacterial attachment.[7,47,49]

While the aforementioned approaches have been shown to confer surfaces with antibacterial properties, the extensive surface fabrication or treatment steps render them to be impractical in terms of cost and labor, widening the gap for these methods to be employed for real-world applications. Herein, we report a novel approach wherein a nanoparticle-based antibacterial coating is directly assembled onto copper surfaces using a simple synthesis procedure. Copper exhibits intrinsic antibacterial properties and is used in a variety of medical devices including dental implants, intrauterine devices, and catheters.[50–55] Copper incorporation into antibacterial coatings and materials has been extensively reviewed by others.[56,57] Using a robust and simple synthesis process, the antibacterial properties of copper are further improved by assembling copper chloride nanoplatelets onto a variety of copper surfaces (**Figure 1**). To the best of our knowledge, this is the first report of assembling nanoparticles on a metal surface using metal ions from the surface itself. The synthesis was conducted by dropping a solution of dilute HCl or dilute HCl in combination with 2 2′-(ethylenedioxy)bis(ethylamine) directly onto the metal surface. The resulting nanoplatelets are referred to as Cu@HCl NP and Cu@HCl-$NH_2$ NP, respectively. The physicochemical properties of the nanoplatelets were extensively characterized, and the improved antibacterial properties of the particle-covered surfaces were compared to those of untreated copper surfaces using data obtained with *Escherichia coli* and multi-drug-resistant (MDR) *E. coli*. These model bacteria were selected because drug resistance in *E. coli* is of increasing concern.[58–62] Further experiments were conducted to explore the antibacterial effects of particle-covered surfaces on other bacteria including MDR *Acinetobacter baumannii*, MDR *Staphylococcus aureus*, and *Streptococcus mutans*. These bacteria were chosen in order to provide a combination of gram-positive, gram-negative, drug-resistant, and regular bacterial strains. The CDC 2019 Antibiotic Resistance Threats Report describes the threat level of methicillin-resistant *S. aureus* and drug-resistant *A. baumannii* as "Serious Threat" and "Urgent," respectively.[63] Thus, by exploring the antibacterial effects of particle-covered surfaces on clinically relevant bacterial strains we aimed to illustrate the potential for the particle-covered surfaces to be used in real-world clinical applications.

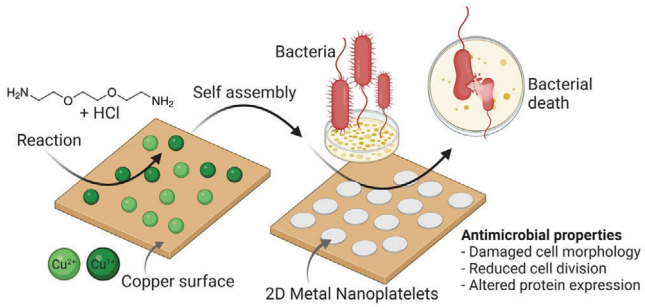


**Figure 1.** Self-assembly of copper-derived nanoplatelets onto copper surfaces. A synthesis solution composed of dilute HCl or dilute HCl in combination with small amounts of 2 2′-(ethylenedioxy)bis(ethylamine) is deposited onto a copper surface and allowed to dry. No copper is present in the synthesis solution itself. Upon deposition of the synthesis solution onto the copper surface, chlorine ions from the HCl couple with copper ions from the surface to form copper chloride crystals (copper nanoplatelets). The nanoplatelets exhibit improved antibacterial properties compared to the copper surfaces alone. The inclusion of 2 2′-(ethylenedioxy)bis(ethylamine) modifies nanoplatelet morphology.

## 2. Results and Discussion

### 2.1. Copper Nanoplatelets Were Assembled Directly on Multiple Copper Surfaces

The precursor solution for Cu@HCl NPs contained only dilute HCl, while the precursor solution for Cu@HCl-$NH_2$ NPs contained dilute HCl and a small amount of 2 2′-(ethylenedioxy)bis(ethylamine) (referred to as diamine). Full details of experimental procedures are provided in Experimental Section. Deposition of the solutions onto the copper side of copper TEM grids led to the formation of nanoplatelets directly on the TEM grid surfaces. TEM imaging revealed the formation of Cu@HCl NPs with sizes of less than 100 nm, in addition to the formation of nanoparticles with diameters less than 10 nm (**Figure 2**A). In contrast, Cu@HCl-$NH_2$ NPs exhibited larger sizes with widths of approximately 0.25 to 1 μm. The rod-like structures in the TEM images provide a view of nanoplatelets with a vertical orientation, confirming that their thickness is in the nanometer range. Additionally, the thin size of the nanoplatelets is also confirmed by the slight reduction in transmission of electrons through areas with overlapping nanoplatelets. The difference in size between Cu@HCl NPs and Cu@HCl-$NH_2$ NPs can be attributed to an effect of diamine on crystallization as the nanoplatelets are formed. The formation of the nanoplatelets on the copper TEM grids was further confirmed by scanning electron microscopy conducted on the TEM grids (Figure 2B and Figure S1, Supporting Information). Some nanoplatelets have either moved from the copper portions of the TEM grid to the carbon surface, or have newly formed on the carbon surface from copper ions that have diffused into the solution from the copper surfaces.

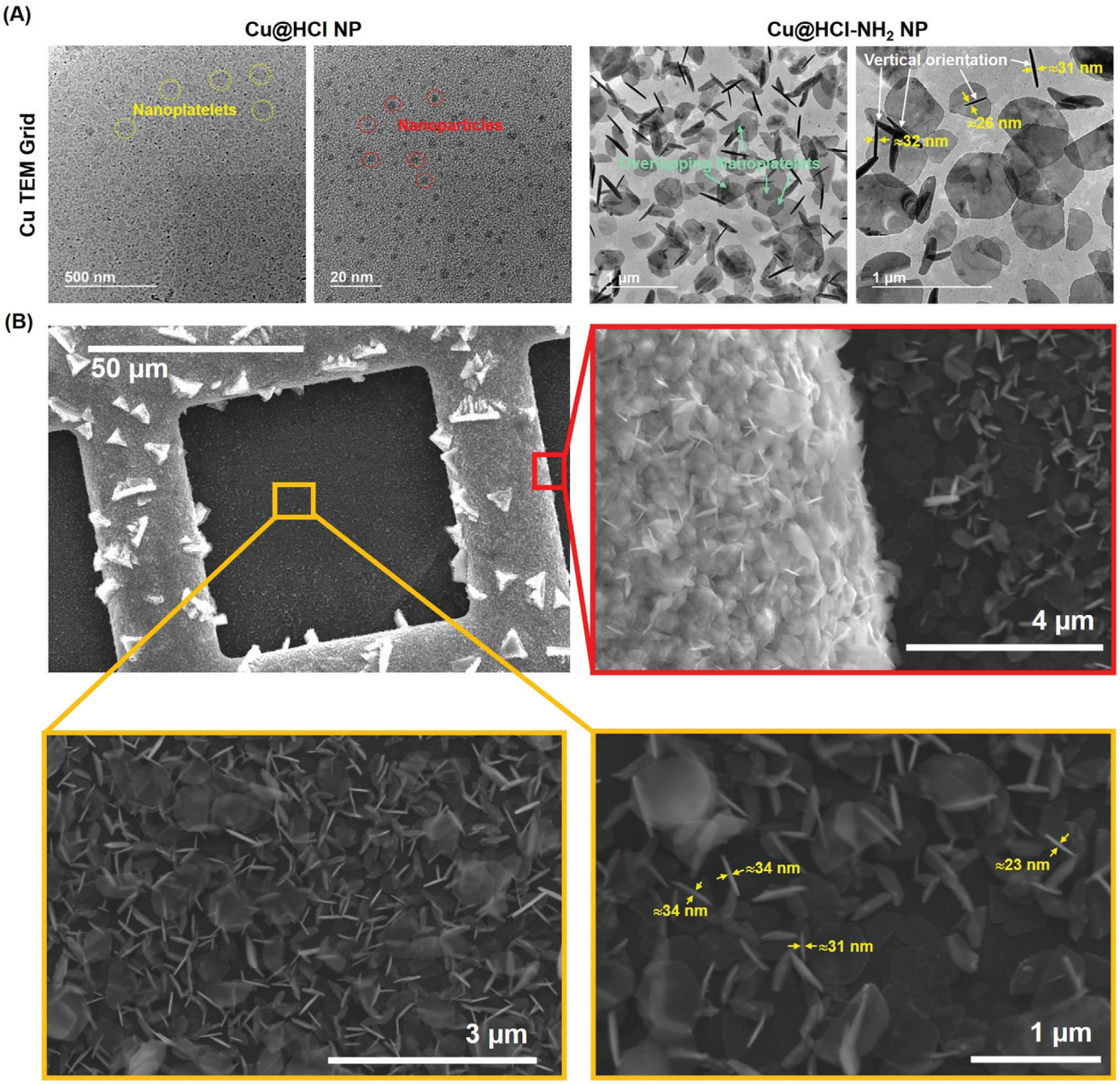


**Figure 2.** Copper chloride nanoplatelets formed on copper TEM grids. A) TEM images of Cu@HCl NPs (left) and Cu@HCl-$NH_2$ NPs (right), formed directly on the copper side of TEM grids (The contrast of the nanoplatelets is less than the contrast from the nanoparticles because the nanoplatelets are very thin). Nanostructures formed using the HCl solution alone include small nanoplatelets and nanoparticles, while the HCl and diamine solution results in the formation of hexagonal nanoplatelets. Rod-like structures are nanoplatelets that are oriented vertically rather than horizontally. B) SEM image of copper grid containing Cu@HCl-$NH_2$ NPs. Nanoplatelets are found both on the copper portion of the grid and on the carbon portion of the grid, indicating the nanoplatelets can either move from the copper surface onto the carbon coating during the synthesis process, or form there from copper ions that have diffused from the copper surfaces.

To confirm the composition of the nanoplatelets, energy dispersive spectroscopy (EDS) was conducted on Cu@HCl-$NH_2$ NPs at various locations on the carbon portion of the TEM grid (Figure S2, Supporting Information). EDS confirmed the presence of copper in these nanoplatelets, and also identified the presence of chlorine atoms, suggesting the nanoplatelets are likely composed of copper chloride. The presence of carbon and oxygen can be attributed to the carbon and oxygen atoms in the carbon grid coating, as well as the atoms in the diamine molecules.

Nanoplatelet precursor solutions were then deposited on copper tape surfaces to form nanoplatelets directly on the copper tape. Scanning electron microscopy images of the tape surfaces reveal the formation of Cu@HCl NPs with widths on the order of micrometers and thicknesses on the order of nanometers, as

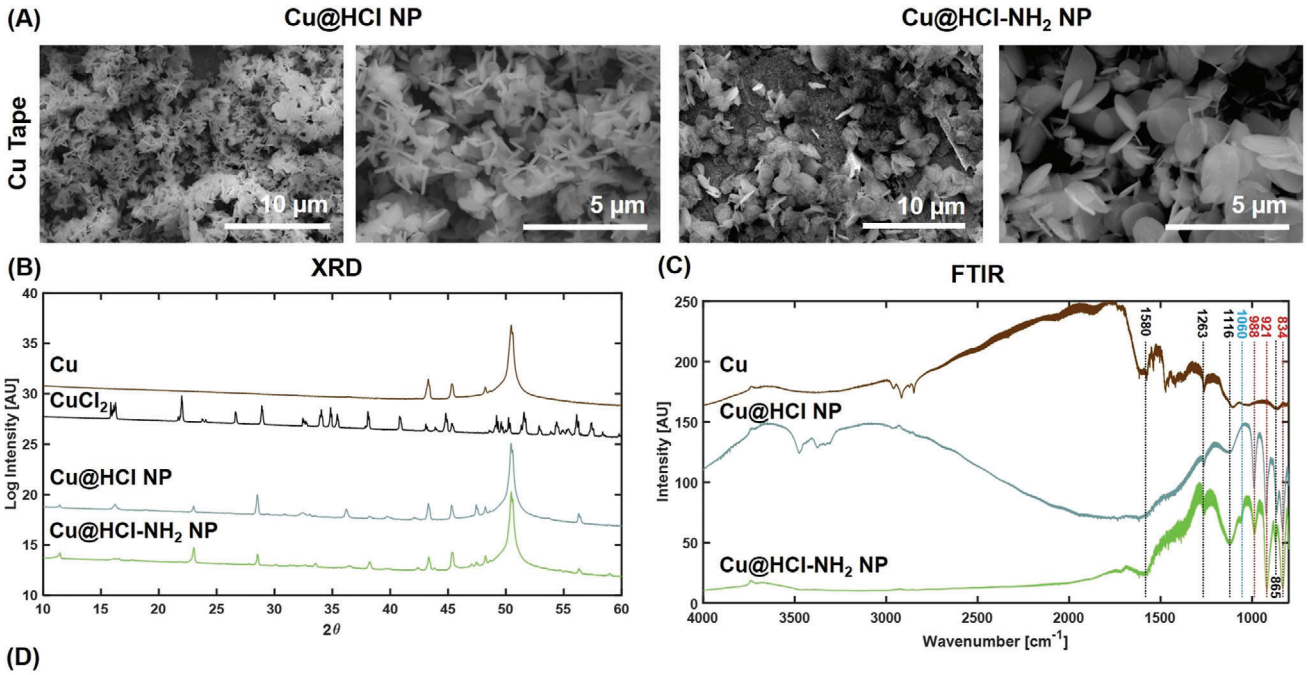


(D)

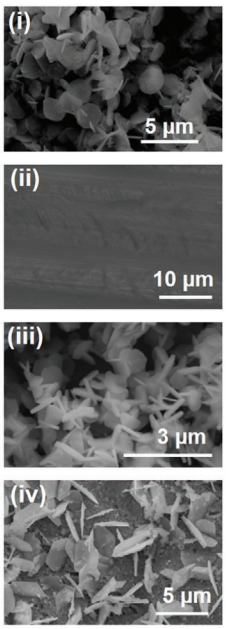


**Effects of Varying Synthesis Parameters on NP Formation**

| Condition | Description | Precursor Solution | | Further dilution before depositing? |
|---|---|---|---|---|
| | | Volume diamine solution (3.5 µL diamine, 10 mL water) | Volume 2N HCl | |
| i | Cu@HCl-$NH_2$ NP (0.35 µL : 50 µL Diamine : HCl ratio) | 1 mL | 50 µL | No |
| ii | No HCl | 1 mL | 50 uL water without HCl | No |
| iii | Cu@HCl NP | 1 mL water without diamine | 50 µL | No |
| iv | Higher Ratio (0.35 µL : 5 µL Diamine : HCl ratio) | 1 mL | 5 µL | No |
| v | Lower Ratio (0.35 µL : 500 µL Diamine : HCl ratio) | 1 mL | 500 µL | No |
| vi | 10 X Less Concentrated | 1 mL | 50 µL | 200 µL precursor solution + 2000 µL water |
| vii | 100 X Less Concentrated | 1 mL | 50 µL | 100 µL of the final dilution for the 10 X Less concentrated condition + 1000 µL water |

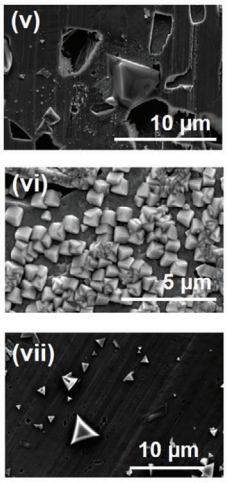


**Figure 3.** Characterization of copper chloride nanoplatelets formed on copper tape. A) SEM images of nanoplatelets formed directly on copper tape: Cu@HCl NPs (left) and Cu@HCl-$NH_2$ NPs (right). B) XRD spectra of copper tape, copper (II) chloride powder, nanoplatelets formed directly on copper tape using the HCl solution, and nanoplatelets formed directly on copper tape using the HCl and diamine solution. C) FTIR spectra of copper tape, Cu@HCl NPs, and Cu@HCl-$NH_2$ NPs formed directly on copper tape. Black lines mark peaks present in Cu, Cu@HCl NPs, and Cu@HCl-$NH_2$ NPs; Red lines mark peaks present in both Cu@HCl NPs and Cu@HCl-$NH_2$ NPs but not in Cu; Blue line marks peak present in only Cu@HCl-$NH_2$ NPs. D) SEM images of results of syntheses carried out under different parameters. Nanoplatelets are only observed in conditions i, iii, and iv. Other shapes were observed when the precursor solution was diluted before being deposited on the copper tape (vi, vii).

well as Cu@HCl-$NH_2$ NPs that are wider than the Cu@HCl NPs (**Figure 3**A). The increase in Cu@HCl-$NH_2$ NP widths can again be attributed to a role of diamine in the nanoplatelet crystallization process. XRD spectra reveal the presence of new peaks in $2\theta$ ranges of 10° to 40° and 55° to 60° for Cu@HCl NPs and Cu@HCl-$NH_2$ NPs, in addition to the peaks in the $2\theta$ range of 40° to 55° that are from the Cu tape itself (Figure 3B). The new peaks that resulted from nanoplatelet formation had some alignment with peaks in the XRD spectra of copper chloride, further suggesting that the nanoplatelets are composed of copper chloride crystals. However, SEM images of commercially obtained Cu(II) chloride powder revealed much larger and irregularly

shaped crystals (Figure S3, Supporting Information), indicating that the nanoplatelets that have been formed on the copper surfaces do not reflect the typical morphology of copper chloride powders, and are instead more ordered in structure. It is important to note that the XRD peaks resulting from copper tape cannot be separated from the signal resulting from the nanoplatelets, as the nanoplatelets are formed directly on copper tape. FT-IR spectra of Cu@HCl NPs and Cu@HCl-$NH_2$ NPs reveal many spectral similarities to that of Cu tape, with the addition of multiple sharp peaks in the 800 $cm^{-1}$ to 1250 $cm^{-1}$ range (Figure 3C). Peaks at approximately 1580, 1263, and 1116 $cm^{-1}$ are observed for Cu tape, Cu@HCl NPs, and Cu@HCl-$NH_2$ NPs. Peaks at approximately 988, 921, and 834 $cm^{-1}$ are observed for Cu@HCl NPs and Cu@HCl-$NH_2$ NPs. A peak at approximately 1060 $cm^{-1}$ is observed for only the Cu@HCl-$NH_2$ NPs. These results suggest high similarity in composition between the Cu@HCl NPs, and Cu@HCl-$NH_2$ NPs. As with the XRD spectra, it is important to note that the FTIR signal resulting from copper tape cannot be separated from the signal resulting from the nanoplatelets, as the nanoplatelets are formed directly on copper tape. Despite these limitations, these results suggest that the nanoplatelets are composed of copper chloride, although it cannot be said with certainty whether they are Cu(I) chloride or Cu(II) chloride. The ability for nanoplatelets to be synthesized on other copper surfaces such as copper electrodes and copper granules was also confirmed with SEM (Figures S4 and S5, Supporting Information).

To evaluate the effects of various synthesis parameters on nanoplatelet formation, syntheses were repeated on copper tape while varying the ratios of diamine to HCl in the precursor solution, in addition to experimenting with different dilutions of the precursor solution prior to deposition on the copper tape (Figure 3D). Nanoplatelets did not form in the absence of HCl (Figure 3D-i), leaving the copper tape surface completely smooth, but formed in the absence of diamine (Figure 3D-iii), confirming the central role of HCl in the nanoplatelet formation process. When the ratio of diamine to HCl was increased 10 times from that used for Cu@HCl-$NH_2$ NP formation (i.e., volume of HCl used was decreased), nanoplatelets still formed but did not appear as regularly shaped as the Cu@HCl NPs or Cu@HCl-$NH_2$ NPs (Figure 3D-iv). When the ratio of diamine to HCl was decreased 10 times from that used for Cu@HCl-$NH_2$ NP formation (i.e., volume of HCl used was increased), we observed the presence of large troughs on the copper tape surface, without nanoplatelet formation (Figure 3D-v). These troughs bear some resemblance to SEM images of metal corrosion and pitting (ref. [64]). This indicates that while an appropriate amount of HCl can lead to the formation of nanostructures, too much HCl may instead lead only to corrosion of the copper tape surface. Indeed, the use of surface treatments to prevent copper corrosion by hydrochloric acid has been the topic of much research.[65–67] When the precursor solution used to form Cu@HCl-$NH_2$ NPs was diluted to a 10 times lower concentration before deposition on the copper tape, cube-shaped structures were formed (Figure 3D-vi). In contrast, when the precursor solution used to form Cu@HCl-$NH_2$ NPs was diluted to a 100 times lower concentration before deposition on the copper tape, triangular structures were observed (Figure 3D-vii). These results suggest that a number of precursor solution concentration windows exist, each of which enables the formation of a different shape. Further exploration of the variety of shapes that can be obtained under different synthesis conditions, as well as evaluation of their potential antibacterial activities, is beyond the scope of this paper, but the present studies revealed a definitive role for HCl in the nanoplatelet synthesis process, in addition to an optimized precursor solution concentration in order to obtain nanoplatelets. Thus, the synthesis conditions that resulted in Cu@HCl-$NH_2$ NPs and Cu@HCl NPs were used for further experiments.

### 2.2. Nanoplatelets Inhibit *E. coli* and MDR *E. coli* Bacterial Growth

To assess the antibacterial properties of the surfaces with copper nanoplatelets compared to those without, an experimental setup was created to enable continuous contact between bacterial suspensions with those surfaces. Cu tape, Cu tape on which Cu@HCl NPs were synthesized, and Cu tape on which Cu@HCl-$NH_2$ NPs were synthesized were adhered to the sides of 24-well plates (**Figure 4**B). Bacterial suspensions were then added to the wells, and optical density at 600 nm (OD600) values representing bacterial concentration was measured over time. The initial color of the surfaces with Cu@HCl-$NH_2$ NPs was observed to be bright green, while those with Cu@HCl NPs exhibited a lighter green color (Figure 4A). With increasing exposure time to the bacterial suspensions, a change in color of both the nanoplatelet tape samples and the suspension was observed (Figure 4A,B). These changes in color include a loss of the green color from the copper tape surfaces, as well as an increase in green color of the bacterial suspensions. These observations suggest that the nanoplatelets are capable of dissolving into the bacterial suspension. Although representative images from a few bacterial strains are provided in Figure 4, similar changes in bacterial suspension color and nanoplatelet tape samples were observed for each bacterial strain tested in these studies.

Changes in bacterial suspension color as a result of nanoplatelet treatment are apparent in both *E. coli* and MDR *E. coli* (Figure 4C,D). The exposure of the broth to nanoplatelet-covered surfaces without bacteria results in the appearance of a UV–visible absorbance peak at 600 nm (Figure S6, Supporting Information). To account for the increase in absorbance at 600 nm due to copper tape with and without nanoplatelets in the absence of bacteria, the OD600 values for broth exposed to Cu tape and Cu tape with nanoplatelets were collected concurrently with, and subtracted from, the OD600 values for the bacteria-containing broth exposed to Cu tape and tape with nanoplatelet samples. In the presence of bacteria, the copper tape led to a smaller increase in OD600 values than when no tape was present at all, indicating a small amount of bacterial growth inhibition. However, the inhibition caused by the surfaces with Cu@HCl NPs and Cu@HCl-$NH_2$ NPs represented a marked improvement over this. The OD600 values after 4 h of bacterial treatment were found to remain almost entirely unchanged for the Cu@HCl NPs and Cu@HCl-$NH_2$ NPs, indicating almost complete inhibition of bacterial growth. This is also apparent in photographs of the well plates after 4 h of treatment, with controls and bacterial suspensions exposed to copper tape having a greater opacity than suspensions exposed to copper tape with nanoplatelets (Figure S7, Supporting Information). Importantly, the final fold

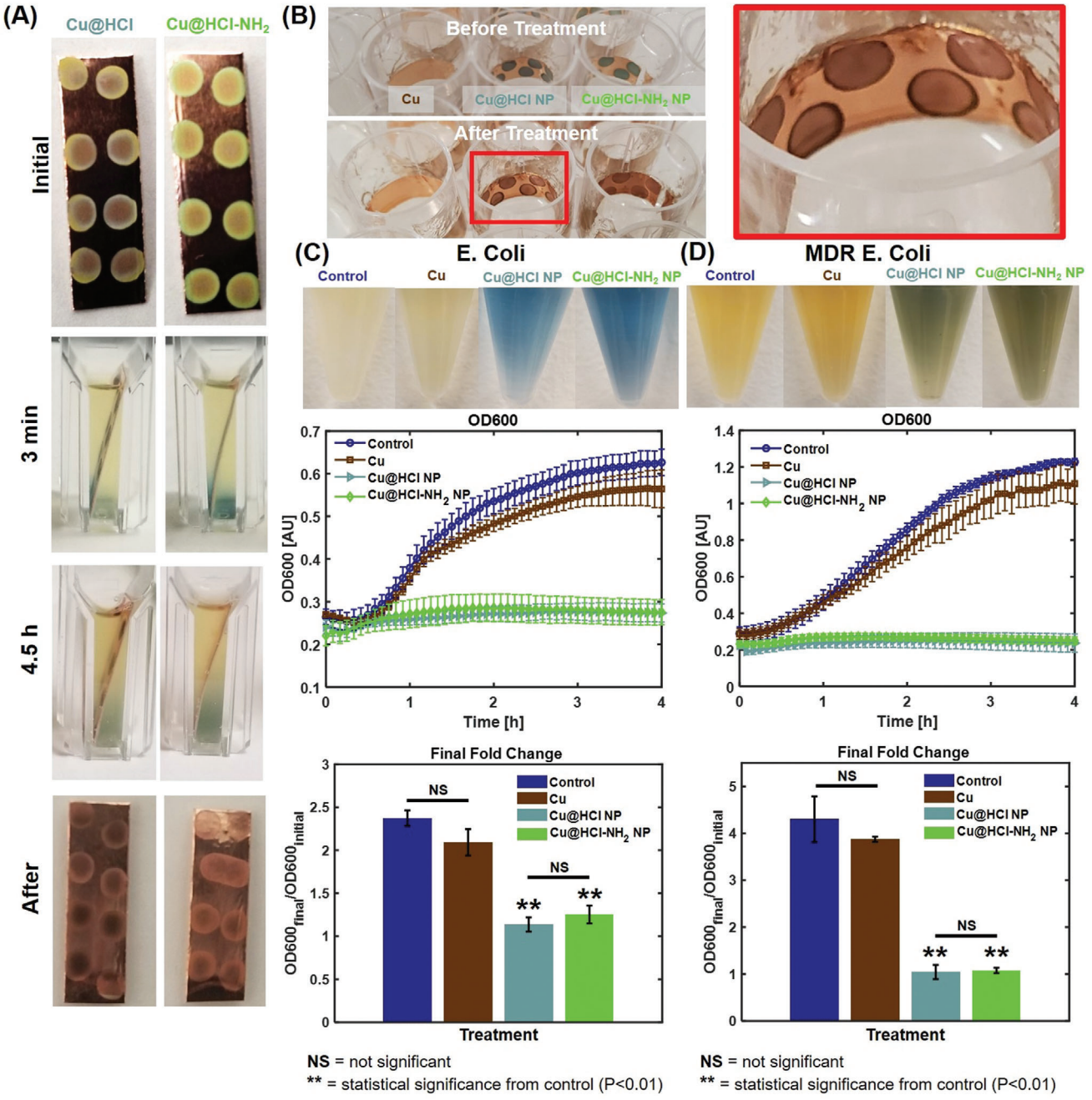


**Figure 4.** Inhibition of bacterial growth by nanoplatelets. A) Representative images of nanoplatelet copper tape samples before, during, and after exposure to *S. mutans* bacteria. A visible color change occurs as a result of nanoplatelet dissolution into the bacterial broth. This was observed with all tested bacterial strains. B) Representative images of samples adhered to wells of 24-well plates. Top panel shows samples before exposure to bacteria, while bottom panel shows samples after exposure to MDR *E. Coli*. This was observed with all tested bacterial strains. C) Growth inhibition of *E. coli* in the presence of nanoplatelets. Nanoplatelets lead to almost complete inhibition of bacterial growth. Values represent averages and error bars represent standard deviations ($n = 8$ for control, $n = 4$ for treatment groups). ** Denotes statistical significance from control, with $P < 0.01$. NS = not significant. Control samples are untreated bacterial suspensions. D) Growth inhibition of MDR *E. coli* in the presence of nanoplatelets. Nanoplatelets lead to almost complete inhibition of bacterial growth. Values represent averages and error bars represent standard deviations ($n = 8$ for control, $n = 4$ for treatment groups). ** Denotes statistical significance from control, with $P < 0.01$. NS = not significant. Control samples are untreated bacterial suspensions.

changes in OD600 values for bacteria treated with nanoplatelet-covered surfaces were very similar for *E. coli* and MDR *E. coli*, even though untreated MDR *E. coli* grew more quickly than *E. coli*. This suggests that the mechanism behind bacterial growth inhibition by the nanoplatelet-covered surfaces is not affected by bacterial drug resistance. This is an important consideration for providing antibacterial options that do not lose efficacy as bacterial strains continue to develop resistance to more antibiotics amongst already-limited antibiotic options. Although nanoparticles can be used for drug delivery, using nanoparticle-based carriers for delivery of antibiotics would be unlikely to help with preventing the further development of bacterial antibiotic resistance. In contrast, the use of particles, such as those described in this work, that are not loaded with antibiotics can provide a potential way in which nanotechnology can be applied to prevent the spread of drug-resistant pathogens.

To ensure that the observed bacterial growth inhibition was not caused by the HCl or HCl-$NH_2$ solutions themselves, experiments were repeated with MDR *E. coli* exposure to liquid HCl solution or HCl-$NH_2$ solution at equivalent concentrations to those used in forming the nanoplatelets (Figure S8, Supporting Information). The results reveal that the solutions themselves have little to no effect on OD600 values, confirming that the observed bacterial growth inhibition is a result of the presence of the nanoparticles on the copper surfaces. The mechanism of growth inhibition is not entirely clear. Considering the toxicity of copper ions,[68,69] the inhibition likely results from the fact that the nanoplatelets increase the surface area from which copper ions can dissolve into the suspension and cause the growth inhibition.

### 2.3. Scanning Electron Microscopy Reveals Bacterial Damage as a Result of Nanoplatelet Treatments

Scanning electron microscopy images were taken of control MDR *E. coli* samples, as well as those treated with Cu, Cu@HCl NPs, and Cu@HCl-$NH_2$ NPs for 4 h (**Figure 5**). Control samples and Cu-treated samples retain a regular rod-like bacterial morphology, while samples exposed to nanoplatelet-covered copper surfaces have altered morphologies. In particular, exposure to those surfaces appears to lead to a wilting and flattening of bacterial samples. This is likely a result of an osmotic imbalance between the concentration of copper ions in the broth and in the bacterial cells. As copper ions are released from the dissolution of nanoplatelets into the bacterial suspension, a high concentration of copper ions would accumulate outside the bacterial cells and lead to hypertonic conditions. In response, the bacterial cells release water in an attempt to regain an equilibrium copper concentration between the bacteria and its environment, leading to the shriveled appearance in cells exposed to platelet-covered surfaces.

Scanning electron microscopy images taken of the tape substrates with which MDR *E. coli* samples were treated (Cu, Cu@HCl NPs, and Cu@HCl-$NH_2$ NPs) demonstrate a low adhesion between the bacterial cells and the copper substrates (**Figure 6**). Furthermore, bacteria on the Cu substrate samples appear to retain their normal rod-like morphology, while those on the nanoplatelet surfaces have a shriveled appearance, further confirming the negative effects of the presence of nanoplatelets on bacterial cell morphology. In addition to the antibacterial effects of the copper ions released by nanoplatelet dissolution into the bacterial suspensions, it is possible that the dissolution of the nanoplatelets acts to prevent bacterial adhesion to the copper surface since bacterial cells may not be able to reach the copper tape surface before coming into contact with dissolved nanoplatelets or those still on the copper tape surface.

### 2.4. Nanoplatelets Also Inhibit *E. Coli* Bacterial Colony Growth

Planktonic culture alone is generally considered inadequate for establishing antibacterial properties due to the fact that bacteria often grow as biofilms on surfaces rather than in a suspension. Thus, antibacterial properties of materials are best explored with further experiments in solid agar-based media that enable bacterial colony growth. To confirm the antibacterial properties of the nanoplatelets in non-planktonic culture we conducted halo tests using an adaptation of previously reported methods.[70] Nanoplatelet-covered copper tape was placed face-down in direct contact with agar plates cultured with *E. Coli*, and the bacterial growth inhibition area was quantified as a function of the substrate area. As can be expected, the antibacterial properties in agar culture were slightly different than those observed in planktonic culture, with the copper tape leading to some apparent inhibition of bacterial colony growth compared to the control untreated condition (**Figure 7**A and Figures S9 and S10, Supporting Information). However, as with the inhibition of bacterial growth in planktonic culture, nanoplatelet-covered surfaces exhibited increased inhibition of bacterial colony growth compared to copper surfaces alone. The growth inhibition area of the nanoplatelet-covered copper surfaces extended to over 200% of the substrate area, while the copper surface growth inhibition area extended to less than 150% of the substrate area. These results further confirm the superior antibacterial properties of the nanoplatelet-covered surfaces compared to the copper surface alone.

### 2.5. Nanoplatelet Planktonic Inhibition of *E. Coli* Growth Extends through 24 h of Contact

To evaluate the ability of nanoplatelet-covered surfaces to inhibit bacterial growth in planktonic conditions over a longer period of time, further well plate experiments were conducted with *E. Coli* over a period of 24 h (Figure 7B). Interestingly, the antibacterial effects of the copper tape appeared to increase between approximately 4 and 8 h of exposure, leading to a drop in bacterial OD600 over this period of time. However, the Cu-treated bacteria then recovered their growth at approximately 10 h of exposure, continuing on to obtain an OD600 value similar to that of the untreated control. This suggests a short-lived delayed antibacterial effect from copper tape, with its effects only becoming apparent after longer-term (>4 h) exposure to the bacteria but fading after a few hours. In comparison, the nanoplatelet-covered surfaces exhibited less bacterial growth than the control or Cu-treated condition for the entirety of the 24 h period, resulting in a significant difference between the final fold changes of bacteria treated for 24 h with nanoplatelet-covered surfaces compared to the

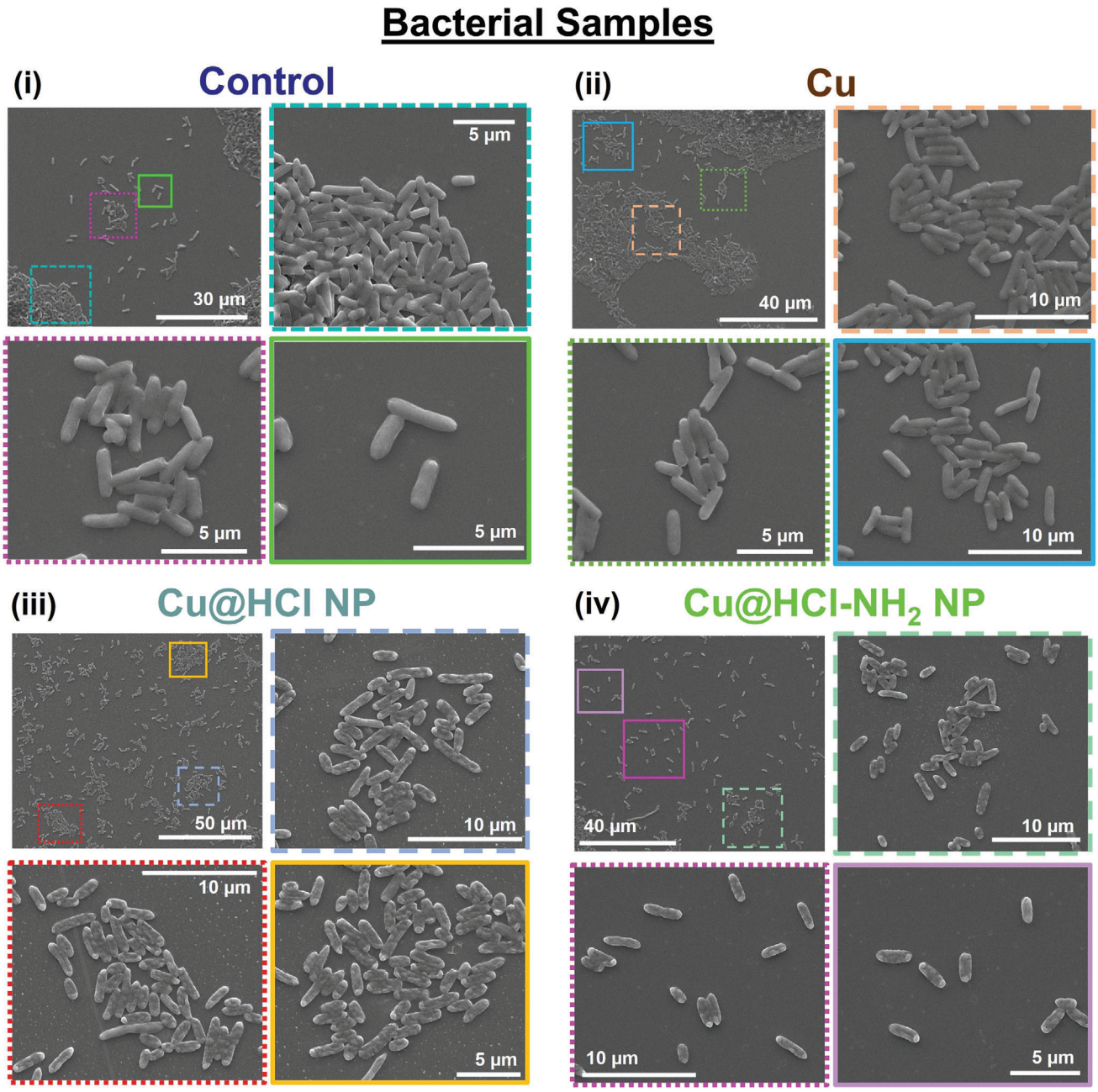


**Figure 5.** Scanning electron microscopy (SEM) images of MDR *E. coli* bacterial samples collected after 4 h of treatment with nanoplatelets. Insets depict higher magnification images of boxed regions. Untreated samples (controls) or samples treated with Cu tape alone exhibit regular bacterial morphologies (i,ii). Samples treated with Cu@HCl NPs or Cu@HCl-$NH_2$ NPs exhibit signs of bacterial damage, including a flattened and shriveled appearance (iii,iv).

untreated control or Cu-treated surfaces. Furthermore, the final fold change in OD600 was less than 1 for Cu@HCl-$NH_2$ NPs (i.e., the final OD600 was less than the initial OD600), indicating that these nanoplatelets not only inhibited bacterial growth but also led to bacterial death over the span of 24 h. Despite there being a higher final fold change in OD600 for the Cu@HCl NPs, the difference between the Cu@HCl-$NH_2$ NPs and the Cu@HCl NPs was not statistically significant. Previous studies have demonstrated important roles for both contact with copper surfaces and exposure to copper ions in copper antibacterial effects.[71] The favorable performance of the nanoplatelet-covered surfaces compared to the copper tape alone can perhaps be linked to the dissolution of the nanoplatelets into either the bacterial broth (planktonic condition) or the solid agar medium (nonplanktonic condition). This dissolution may lead to a "burst release" of copper ions and therefore the nanoplatelet antibacterial effects, enabling the prevention of bacterial growth from early on in bacterial exposure to the antibacterial surfaces. The

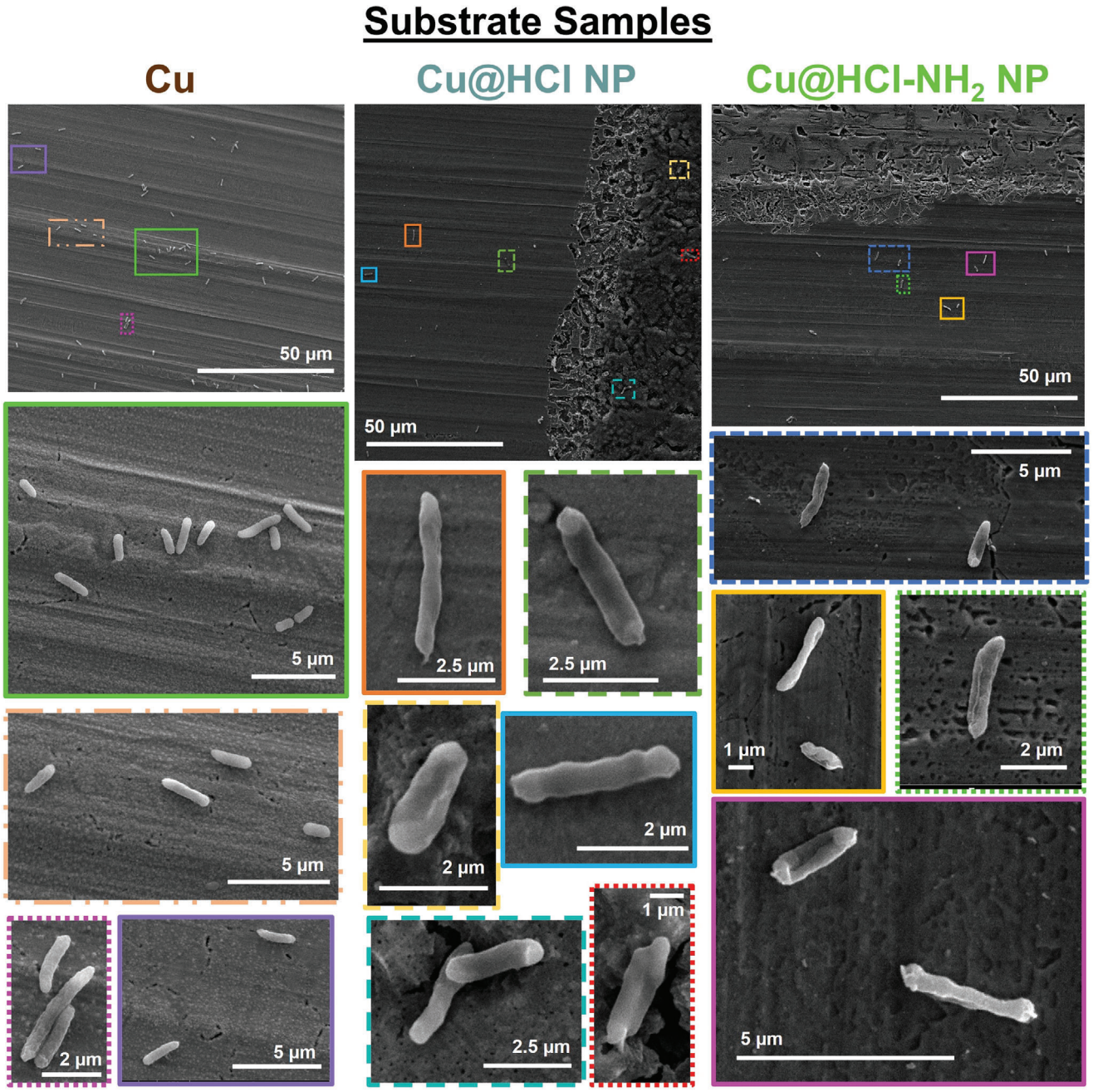


**Figure 6.** Scanning electron microscopy (SEM) images of MDR *E. coli* on copper substrates after 4 h of treatment. Insets depict higher magnification images of boxed regions. Bacteria treated with copper alone exhibit relatively normal morphologies, and exhibit some adhesion to the copper surface. Bacteria treated with nanoplatelets have minimal adhesion to the surface, and exhibit signs of damage.

nanoplatelet-covered surfaces may provide a greater initial surface area to facilitate short-lived direct contact between the bacterial suspension and the copper surface, as well as providing a greater surface area for copper ion dissolution into the bacterial suspension. On the other hand, the inability of the Cu surface itself to exhibit a strong immediate antibacterial effect may be due to slower or non-occurrence of copper ion release by the Cu surface, as well as a smaller surface area for bacterial contact compared to the nanoplatelet-covered surfaces.

### 2.6. Nanoplatelets Exhibit Antibacterial Effects on Other MDR and Regular Bacterial Strains

Two further MDR bacterial strains were selected for planktonic analysis of antibacterial activities. Methicillin-resistant *S. aureus* (MRSA) is a common gram-positive bacteria that spread in healthcare facilities, leading to challenges with treatment due to its antibiotic resistance.[63] MRSA is listed as a "Serious Threat" in the CDC 2019 "Antibiotic Resistance Threats In the

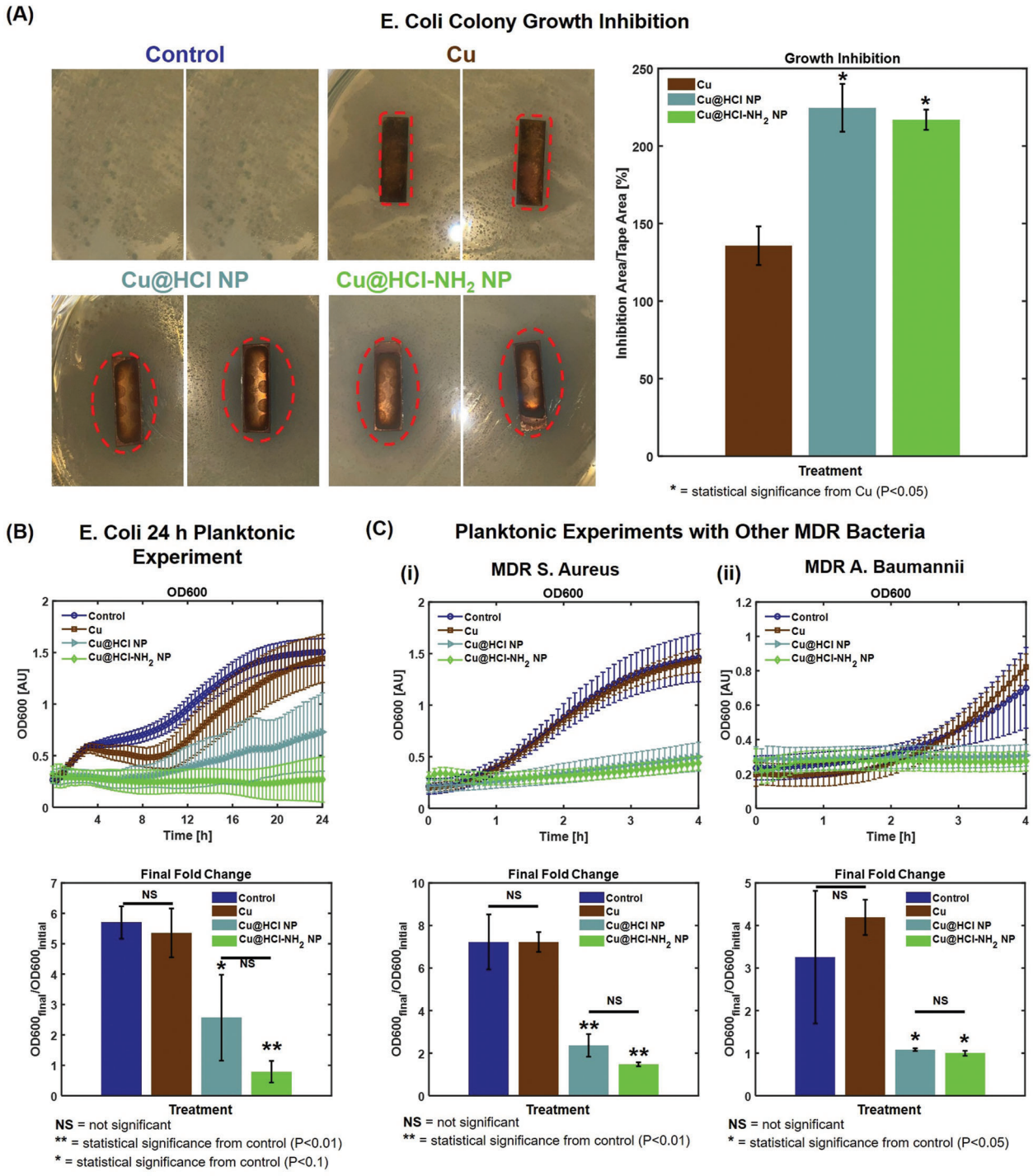


**Figure 7.** Further exploration of antibacterial properties of nanoplatelet-covered surfaces. A) Halo test in which nanoplatelet-covered copper surfaces were exposed for 24 h to nonplanktonic *E. coli* grown in agar medium. Inhibition of bacterial colony growth was observed for samples treated with Cu, Cu@HCl NPs, and Cu@HCl-$NH_2$ NPs, but inhibition was significantly higher for the nanoplatelet-treated samples. Red dashed lines provide a sample outline of the inhibition area for each sample. Data are represented as an average of 2 samples on a single plate for each condition, with error bars representing standard deviation. * Denotes statistical significance from Cu, with $P < 0.05$. B) Planktonic growth inhibition of *E. coli* in the presence of nanoplatelets for 24 h. Nanoplatelets significantly reduce bacterial growth. Values represent averages and error bars represent standard deviations ($n = 4$ for each group). ** Denotes statistical significance from control, with $P < 0.01$. * Denotes statistical significance from control with $P < 0.1$. NS = not significant. Control samples are untreated bacterial suspensions. C) Planktonic growth inhibition of MDR *S. aureus* and MDR *A. baumannii*. Nanoplatelets significantly reduced bacterial growth for both types of bacteria. Control samples are untreated bacterial suspensions. Values represent averages and error bars represent standard deviations. (i) $n = 8$ for control, $n = 4$ for treatment groups). ** Denotes statistical significance from control, with $P < 0.01$. NS = not significant. (ii) $n = 7$ for control, $n = 3$–4 for treatment groups. * Denotes statistical significance from control, with $P < 0.05$.

United States" report. MRSA has been found on a variety of surfaces in hospital settings.[72,73] The *S. aureus* strain we used in these studies is resistant to multiple drugs, including methicillin. *A. baumannii* is a gram-negative bacteria that can survive for an extended period of time on surfaces, and the occurrence of carbapenem-resistant Acinetobacter infections in patients in healthcare facilities is a major concern as it can lead to pneumonia and infections in wounds, the bloodstream, and the urinary tract.[63] Carbapenem-resistant Acinetobacter is listed as an "Urgent Threat" in the CDC 2019 "Antibiotic Resistance Threats In the United States" report. The strain we used in these studies is resistant to many drugs including carbapenems Imipenem, and Meropenem.[74]

Over a 4 h treatment period, the OD600 values of *S. aureus* treated with copper tape tracked closely with those of untreated *S. aureus* (Figure 7C-i). In contrast, *S. aureus* exposed to Cu@HCl NPs or Cu@HCl-$NH_2$ NPs had a much slower increase in OD600 values. *S. aureus* that was untreated or treated with copper tape exhibited a greater than sevenfold change in OD600 values after 4 h, while *S. aureus* that was treated with Cu@HCl NPs or Cu@HCl-$NH_2$ NPs had a less than threefold change in OD600 values over the same time period. For *A. baumannii*, little to no change in bacterial OD600 values was observed for the first two hours, indicating possible slow bacterial growth. However, after approximately two hours an increase in OD600 values is observed for untreated bacteria and bacteria treated with copper tape (Figure 7C-ii). Little to no change in OD600 values is observed for *A. baumannii* treated with Cu@HCl NPs or Cu@HCl-$NH_2$ NPs over the entirety of the 4 h treatment period, and the fold change for both Cu@HCl NPs and Cu@HCl-$NH_2$ NPs was close to 1. These experiments demonstrate the capability of the nanoplatelet-covered surfaces to slow bacterial growth of multiple strains of drug-resistant bacteria that have been associated with hospital infections.

To further explore the antibacterial properties of the nanoplatelet-covered surfaces against gram-positive bacteria, experiments were conducted using *S. mutans*, a strain of gram-positive bacteria associated with dental plaque and caries.[75] Here again, the OD600 values of control bacteria and copper-treated bacteria tracked closely with each other, while the OD600 values of the nanoplatelet-treated bacteria rose at a slower rate (Figure S11, Supporting Information). Overall, these experiments confirm that the effects of the nanoplatelet-covered surfaces are not restricted to a single bacterial strain, but instead extend to gram-positive and gram-negative bacteria, in addition to extending to multiple strains of drug-resistant bacteria.

### 2.7. Exposure to Nanoplatelet-Covered Copper Surfaces Reduced Bacterial Viability and Induced DNA Damage

Multiple studies were conducted to determine the mechanism by which the presence of nanoplatelets inhibits bacterial growth. Although OD600 measurements can provide information on the concentration of bacteria, they do not provide a direct measure of cell viability. To assess the viability of treated cells, live-dead staining of MDR *E. coli* was conducted using a commercial green stain for live cell indicator (live cell indicator) and propidium iodide (dead cell indicator), where a lower ratio of green to red fluorescence would indicate lower viability (**Figure 8**A). These studies demonstrated that the presence of nanoplatelet-covered copper surfaces not only inhibit bacterial cell division, but also reduced bacterial cell viability within only 4 h of exposure. This result is consistent with copper ion toxicity observed by others.[68]

Since cell division appeared to be affected by the presence of nanoplatelet-covered copper surfaces, terminal deoxynucleotidyl transferase dUTP nick end labeling (TUNEL) assays were conducted to identify DNA damage in the bacterial samples (Figure 8B). In TUNEL assays, fragmented DNA is labeled with a fluorescent dye, and the presence of greater DNA fragmentation leads to a greater fluorescent intensity. Cu alone was found to lead to some DNA fragmentation, as can be expected from the antibacterial properties of Cu. However, the presence of Cu@HCl NPs and Cu@HCl-$NH_2$ NPs led to greater DNA fragmentation than the Cu treatment alone, confirming that the nanoplatelets provide a mechanism leading to a more potent antibacterial function. To further confirm this, gel electrophoresis was conducted on genomic DNA extracted from bacterial control samples, as well as bacterial samples treated with Cu, Cu@HCl NPs, and Cu@HCl-$NH_2$ NPs (Figure 8C). Exposure to nanoplatelet-covered surfaces reduced DNA band intensity for both *E. coli* and MDR *E. coli*, while untreated control samples and samples treated with Cu surfaces alone exhibited high band intensities, further confirming the role of nanoplatelets in preventing bacterial cell division by inducing DNA damage.

To determine whether the nanoplatelets generated reactive oxygen species (ROS) that led to the DNA damage, ROS generation assays were conducted using CM-$H_2$DCFDA, a fluorescent ROS indicator that has high retention in cells, enabling long-term studies. CM-$H_2$DCFDA was loaded into MDR *E. coli* samples, and the fluorescence intensity of the bacterial samples was monitored every 5 min for 4 h, with a greater fluorescence intensity corresponding to a higher presence of ROS. Although Cu alone was found to lead to some ROS generation near the beginning of the treatment, the presence of nanoplatelets on the copper surface was found to lead to lower fluorescence intensity than the control (Figure S12, Supporting Information). This indicates that the nanoplatelets may in fact be acting as ROS scavengers rather than inducing ROS generation. To ensure that this observation was not a result of CM-$H_2$DCFDA photobleaching with time, the experiment was repeated with bacterial samples protected from light during the experiment, and measurements were collected only after 4 h of treatment (Figure S13, Supporting Information). This further confirmed that ROS generation is not the mechanism by which nanoplatelet-induced DNA fragmentation occurred. Our results are consistent with those of Park et al., who found that copper ions do not increase hydroxyl radical production and may even reduce superoxide levels.[69]

### 2.8. Exposure to Nanoplatelet-Covered Copper Surfaces Led to Changes in Bacterial Protein Expression

In addition to evaluating DNA damage caused by the presence of nanoplatelets, further studies were conducted to evaluate the effects of nanoplatelet-covered copper surfaces on bacterial protein expression. Water-soluble proteins were extracted from

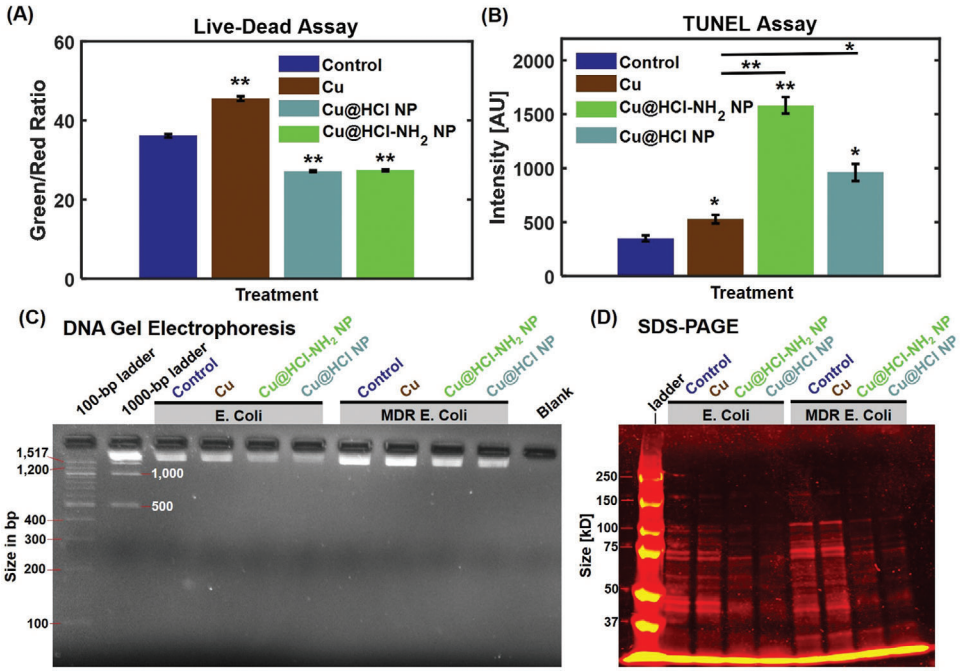


**Figure 8.** Exploration of mechanisms behind bacterial growth inhibition by nanoplatelets. A) Live–dead assay conducted on MDR *E. coli* treated with samples for 4 h. A higher green/red ratio indicates greater cell viability. A reduction in cell viability is caused by the nanoplatelet treatments. Values represent averages and error bars represent standard deviations across three technical replicates. ** indicates statistical significance with $P < 0.01$. B) TUNEL assay conducted on MDR *E. coli* treated with samples for 4 h. A higher intensity indicates a greater level of DNA damage. Nanoplatelets induce greater DNA damage than Cu alone. Values represent averages and error bars represent standard deviations across three technical replicates. Asterisks over individual bars indicate statistical significance with respect to the control. ** indicates statistical significance with $P < 0.01$, * indicates statistical significance with $P < 0.05$. C) Gel electrophoresis results for genomic DNA extracted from *E. coli* and MDR *E. coli* treated with samples for 4 h. Reductions in band intensities for Cu@HCl NP-treated and Cu@HCl-$NH_2$ NP-treated samples confirm DNA damage induced by the nanoplatelets. These differences are apparent in both *E. coli* and MDR *E. coli*. D) SDS-PAGE results for proteins extracted from *E. coli* and MDR *E. coli* treated with samples for 4 h. Nanoplatelets lead to reductions in band intensities, and in some cases complete removal of some protein bands, indicating that they have changes in protein expression. These changes are apparent in both *E. coli* than in MDR *E. coli*.

untreated control samples, as well as bacteria exposed to copper surfaces, Cu@HCl NPs, and Cu@HCl-$NH_2$ NPs. SDS PAGE was conducted on these protein samples (Figure 8D) and demonstrates a clear difference in protein expression for nanoplatelet-treated bacteria compared to Cu-treated or untreated bacteria. These changes in protein expression are apparent for both *E. coli* and MDR *E. coli*. Furthermore, exposure to copper surfaces without nanoplatelets appeared to lead to little change in protein expression in either type of bacteria.

To examine this in greater detail, proteomic analysis was carried out to identify individual proteins present in the protein population extracted from the bacteria. Heatmaps were created using the -10logP values for all detected proteins for *E. coli* and MDR *E. coli*, where a higher -10log*P* value corresponds to a greater confidence in the identification of the proteins. In this work, we have divided -10log*P* values into 3 ranges: values greater than 75 are considered the identification of the proteins with high confidence, values between 45 and 75 are considered the identification of the proteins with acceptable confidence, and values below 45 are considered proteins that cannot be confidently identified in the samples. A list of all protein IDs and their corresponding protein Accession IDs and descriptions are provided in Tables S1 and S2 (Supporting Information).

### *2.8.1. Proteomic Analysis of MDR E. coli*

There were fewer identified proteins in MDR *E. coli* samples exposed to copper surfaces without nanoplatelets (450 proteins), Cu@HCl-covered copper surfaces (130 proteins), and Cu@HCl-$NH_2$-covered copper surfaces (182 proteins) than in control samples that were not exposed to any of the surfaces (577 proteins). This confirms SDS PAGE observations which illustrated that exposure to nanoplatelet-covered Cu surfaces had a major impact on protein expression.

A heatmap of identified proteins in the MDR *E. coli* samples is provided in **Figure 9**A. Three proteins related to cell division were identified in the control sample: 89 (P0A9A6|FTSZ_ECOLI, Cell division protein FtsZ), 630 (P0AF36|ZAPB_ECOLI, Cell division protein ZapB), and 734 (P45955|CPOB_ECOLI, Cell division coordinator CpoB). Protein 89 was identified with lower -10log*P* values in bacterial samples treated with Cu, Cu@HCl NPs, or Cu@HCl-$NH_2$ NPs, and protein 734 could not be confidently identified in these samples. A downregulation of cell division proteins as a result of treatment can be directly related to the lack of cell division observed during the OD600 measurements.

Additionally, protein 78 (Q59385|COPA_ECOLI, Copper-exporting P-type ATPase) was identified in MDR *E. coli* treated

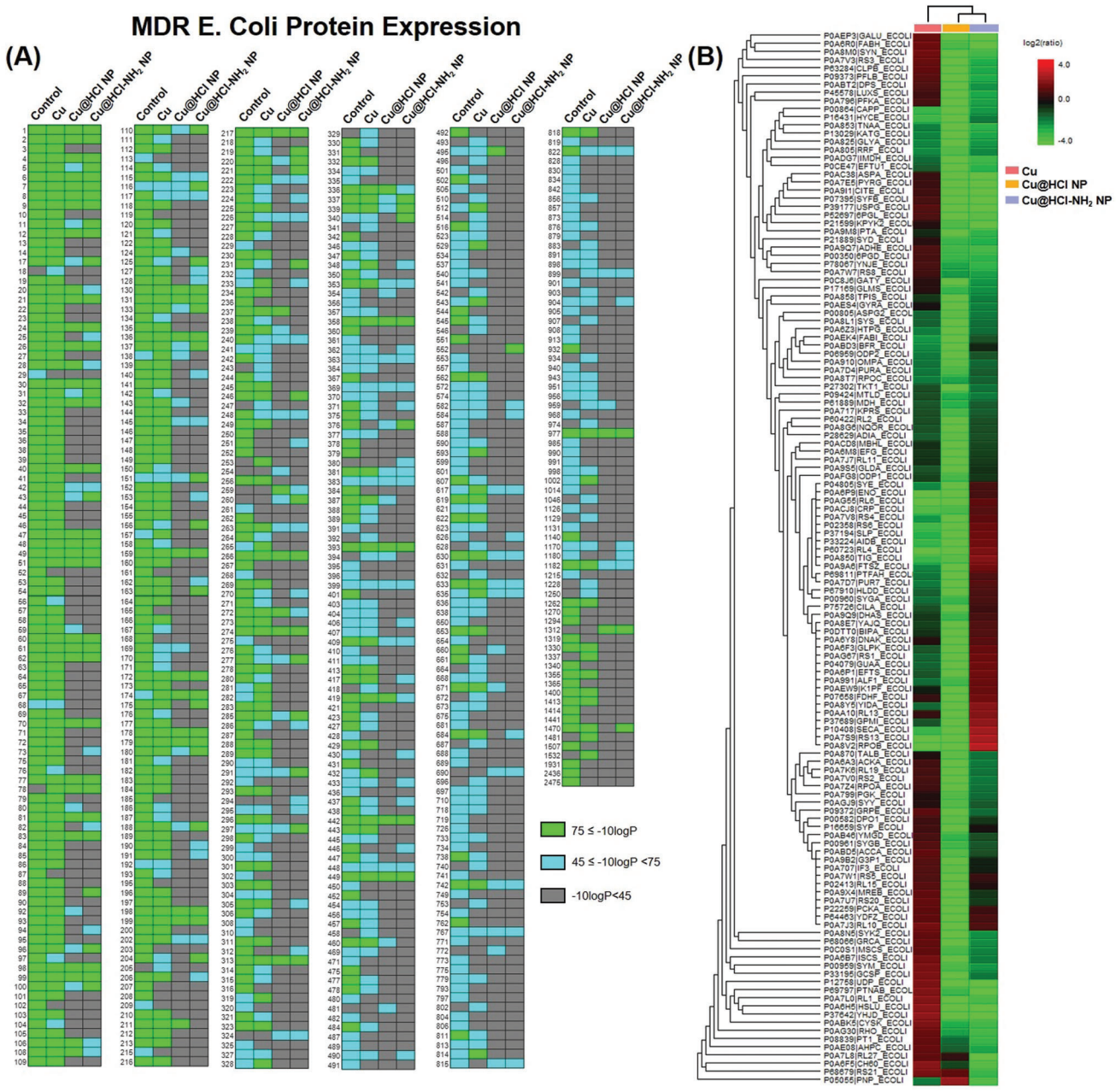


**Figure 9.** Proteomics analysis of MDR *E. coli*. A) Heat maps classifying the -10log*P* values of each protein in each sample. Data represent a compilation of three technical replicates taken from each sample. B) Hierarchical clustering of ratios between protein relative expression in each sample and protein relative expression in the control sample. Data represent the most data-rich technical replicate of three technical replicates for each sample.

with either Cu or nanoplatelets, but not in the control sample. Protein 458 (P36649|CUEO_ECOLI, blue copper oxidase), a protein believed to be involved in the detoxification of copper, was also identified in Cu-treated samples, but not in the control or the nanoplatelet-treated samples. Thus, the DNA damage caused by exposure to nanoplatelet-coated copper surfaces may have prevented the eventual synthesis of some of the proteins that would provide the MDR *E. coli* with copper tolerance. In contrast, exposure to uncoated Cu surfaces may have led to the synthesis of proteins that would increase the copper tolerance of MDR *E. coli*.

We further examined proteins related to DNA. Protein 58 (P0AES4|GYRA_ECOLI, DNA gyrase subunit A), which is known to be involved in ATP-dependent breakage, passage, and rejoining of double-stranded DNA, and therefore plays a role in its transcription, repair, and replication, is present in the control sample and Cu-treated sample, but not in the nanoplatelet-treated samples. Protein 90 (P00582|DPO1_ECOLI, DNA polymerase I) is also present in the control samples and samples exposed to uncoated copper surfaces, but not in those exposed to nanoplatelet-coated copper surfaces. This protein

**Table 1.** Proteins of interest in MDR *E. coli* samples.

| Protein ID | Accession ID | Description | Observation |
|---|---|---|---|
| 734 | P45955\|CPOB_ECOLI | Cell division coordinator CpoB | Not identified in treated samples |
| 78 | Q59385\|COPA_ECOLI | Copper-exporting P-type ATPase | Identified in treated samples but not in control |
| 458 | P36649\|CUEO_ECOLI | Blue copper oxidase | Identified in Cu-treated samples but not control or nanoplatelet-treated samples |
| 410 | P06612\|TOP1_ECOLI | DNA topoisomerase 1 | Not identified in treated samples |
| 1215 | P12295\|UNG_ECOLI | Uracil-DNA glycosylase | |
| 58 | P0AES4\|GYRA_ECOLI | DNA gyrase subunit A | Not identified in nanoplatelet-treated samples |
| 90 | P00582\|DPO1_ECOLI | DNA polymerase I | |
| 114 | P0AES6\|GYRB_ECOLI | DNA gyrase subunit B | |

exhibits polymerase and exonuclease behaviors. Protein 114 (P0AES6|GYRB_ECOLI, DNA gyrase subunit B), which relaxes negatively supercoiled DNA, is identified with less confidence in the sample exposed to Cu surfaces than the control samples, and is not confidently identified in the samples exposed to nanoplatelet-covered Cu surfaces. Proteins 410 (P06612|TOP1_ECOLI, DNA topoisomerase 1) and 1215 (P12295|UNG_ECOLI, Uracil-DNA glycosylase) could not be confidently identified in any of the treated samples, despite being identified in the control sample. These proteins are responsible for ATP-independent breakage of single-stranded DNA and releasing uracil residues respectively. Finally, protein 529 (P0ABE2|BOLA_ECOLI, DNA-binding transcriptional regulator BolA), which is known to have an impact on cell morphology, cell growth, and cell division, is identified in the control and Cu-exposed samples, but not confidently identified in the samples exposed to nanoplatelet-coated surfaces. Altogether, these results confirm that the exposure to nanoplatelet-covered surfaces had an impact on MDR *E. coli* cell division, response to copper, and DNA replication (**Table 1**).

To develop an understanding of each sample's protein expression relative to the control sample, the ratio of each protein's ion counts to the total ion counts for each sample was calculated. This relative expression ratio was then divided by the relative expression ratio of the same proteins in the control sample. This enabled a comparison between the relative abundance of different proteins in the treated samples compared to the untreated control. Hierarchical clustering of these protein ratios identified similarities between samples exposed to nanoplatelet-covered surfaces compared to the samples exposed to copper surfaces without nanoplatelets (Figure 9B). In addition, the presence of nanoplatelets generally led to decreased expression of many proteins, while the absence of nanoplatelets on copper surfaces led to increased expression of some proteins critical to survival. For example, Cu-treated samples had an increased relative expression (compared to the control) of P0ABT2|DPS_ECOLI, which is responsible for protecting the bacterial cells from copper ion toxicity.

### *2.8.2. Proteomic Analysis of E. coli*

As for MDR *E. coli*, there are fewer proteins in the *E. coli* samples treated with Cu (377 proteins), Cu@HCl NPs (178 proteins), and Cu@HCl-$NH_2$ NPs (110 proteins) compared to the untreated control (611 proteins). This further confirms the *E. coli* SDS PAGE observations which illustrated that the presence of nanoplatelets had a major impact on protein expression.

A heatmap of identified proteins in the *E. coli* samples is provided in Figure S14A (Supporting Information). A number of proteins related to cell division were identified in the control sample. Protein 89 (P0A9A6|FTSZ_ECOLI, Cell division protein FtsZ), which is responsible for forming a contractile ring structure (Z ring) at the future cell division site, was identified with high confidence in both the control and Cu-treated samples, but was identified with lower confidence in Cu@HCl NP-treated copper surfaces and could not be confidently identified in sample exposed to Cu@HCl-$NH_2$ NP-treated copper surfaces. Protein 900 (P0A734|MINE_ECOLI, Cell division topological specificity factor), which is responsible for ensuring the occurrence of cell division at the proper site, was identified in the control sample but not in the treated samples.

A number of proteins related to DNA were also altered in expression as a result of the exposure to copper surfaces. Protein 260 (P0ACF0|DBHA_ECOLI, DNA-binding protein HU-alpha), protein 265 (P0A800|RPOZ_ECOLI, DNA-directed RNA polymerase subunit omega), protein 272 (P0ACG1|STPA_ECOLI, DNA-binding protein StpA), protein 402 (P23909|MUTS_ECOLI, DNA mismatch repair protein MutS), protein 528 (P0ACB0|DNAB_ECOLI, Replicative DNA helicase), protein 837 (P21189|DPO2_ECOLI, DNA polymerase II), protein 1250 (P0ABS5|DNAG_ECOLI, DNA primase), and protein 1294 (P65556|YFCD_ECOLI, DNA primase) were all identified in the control sample but could not be confidently identified in any of the samples exposed to any of the copper surfaces (both coated and uncoated with nanoplatelets). Proteins 80 (P0A7Z4|RPOA_ECOLI, DNA-directed RNA polymerase subunit alpha), 85 (P0A9 × 4|MREB_ECOLI, DNA-directed RNA polymerase subunit omega), 86 (P04805|SYE_ECOLI, DNA-directed RNA polymerase subunit alpha), 90 (P00582|DPO1_ECOLI, DNA polymerase I), 114 (P0AES6|GYRB_ECOLI, DNA gyrase subunit B), and 529 (P0ABE2|BOLA_ECOLI, DNA-binding transcriptional regulator BolA) were all identified in the control and Cu-treated samples but not in the samples exposed to nanoplatelet-covered surfaces (**Table 2**).

Hierarchical clustering of *E. coli* protein ratios identified similarities between the samples exposed to nanoplatelet-covered surfaces compared to the samples exposed to bare copper surfaces (Figure S14B, Supporting Information). As with MDR

**Table 2.** Proteins of interest in *E. coli* samples.

| Protein ID | Accession ID | Description | Observation |
|---|---|---|---|
| 89 | P0A9A6\|FTSZ_ECOLI | Cell division protein FtsZ | Identified with high confidence in control and Cu-treated samples, lower confidence in Cu@HCl NP-treated samples, and not identified in Cu@HCl-$NH_2$ NP-treated samples |
| 900 | P0A734\|MINE_ECOLI | Cell division topological specificity factor | Not identified in treated samples |
| 260 | P0ACF0\|DBHA_ECOLI | DNA-binding protein HU-alpha | |
| 265 | P0A800\|RPOZ_ECOLI | DNA-directed RNA polymerase subunit omega | |
| 272 | P0ACG1\|STPA_ECOLI | DNA-binding protein StpA | |
| 402 | P23909\|MUTS_ECOLI | DNA mismatch repair protein MutS | |
| 528 | P0ACB0\|DNAB_ECOLI | Replicative DNA helicase | |
| 837 | P21189\|DPO2_ECOLI | DNA polymerase II | |
| 1250 | P0ABS5\|DNAG_ECOLI | DNA primase | |
| 1294 | P65556\|YFCD_ECOLI | DNA primase | |
| 80 | P0A7Z4\|RPOA_ECOLI | DNA-directed RNA polymerase subunit alpha | Not identified in nanoplatelet-treated samples |
| 85 | P0A9 × 4\|MREB_ECOLI | DNA-directed RNA polymerase subunit omega | |
| 86 | P04805\|SYE_ECOLI | DNA-directed RNA polymerase subunit alpha | |
| 90 | P00582\|DPO1_ECOLI | DNA polymerase | |
| 114 | P0AES6\|GYRB_ECOLI | DNA gyrase subunit B | |
| 529 | P0ABE2\|BOLA_ECOLI | DNA-binding transcriptional regulator BolA | |

*E. coli*, exposure to nanoplatelets generally led to decreased expression of many proteins, while exposure to Cu surfaces without nanoplatelets led to increased expression of many proteins critical to survival. These findings further confirm the role of the presence of nanoplatelets in modulating protein expression.

### 2.9. Nanostructures Were Also Assembled Directly on Multiple Other Metal Surfaces

To determine whether nanoplatelets could be assembled on other metal surfaces, the synthesis procedures were repeated by depositing the HCl solution or HCl and diamine solution onto pieces of tin, zinc, and cobalt and allowing the solution to dry. Scanning electron microscopy was then conducted on the samples (Figures S15 and S16, Supporting Information). These images revealed the successful formation of nanostructures on these various metal surfaces. Although the structures differed in shape from one metal type to another, these results suggest a simple aqueous solution containing acid can be applied to metal surfaces to obtain textured nanoscale patterns and structures on the surfaces. The goal in conducting experiments on these other metal surfaces was to determine whether nanostructures could be easily assembled onto metal surfaces not composed of copper, potentially for other applications aside from antibacterial applications. In fact, tin has been shown to not have antibacterial properties.[76] Additionally, the relative stiffness of these metal surfaces compared to the flexible copper tape substrates we used in the bacterial experiments above make them unamenable to testing in the 24-well experimental setup we have created to enable continuous contact between planktonic bacterial suspensions and the metal surfaces. Thus, experiments to evaluate the antibacterial properties of the nanostructures on these other metal surfaces are out of the scope of this present work.

### 2.10. Comparison of Nanoplatelets with Other Antibacterial Surfaces

Comparing the performance of the nanoplatelets described in this work with that of other antibacterial surfaces described by other researchers is challenging due to the differences in experimental methods and relative synthetic complexity of many antibacterial surfaces. However, some general comparisons regarding synthetic simplicity, morphological controllability, and antibacterial efficacy can be made.

One example of a flexible antibacterial film was developed by Wang et al.[77] In their work, silver nanoparticles were formed on a poly(dimethylsiloxane) surface by immersion in $Ag(NH3)_2OH$ followed by immersion in glucose. Afterward, the film was sequentially dipped in solutions of poly(l-lysine) and poly(acrylic acid), followed by coating with a cationic conjugated polyelectrolyte, poly({9,9-bis[6′-(N,N-trimethylamino)hexyl]-2,7-fluorenyleneethynylene}-alt-co-1,4-(2,5-dimethoxy)phenylene)dibromide (PFEMO), which served as a light-activated antibacterial agent. They evaluated the antibacterial properties of their material by adding the bacterial solution to the substrate, treating it with white light for 5 min as applicable, and then spreading the bacterial solution on a solid agar plate and counting the colony-forming units (CFUs) after 12 h of incubation. When samples were treated with light, they observed a 99% killing efficiency when Ag and PFEMO were both incorporated in the films, and a 41% killing efficiency when PFEMO was incorporated without Ag. However, the killing efficiency was lower when Ag was incorporated without PFEMO, as well as for all conditions when samples were not treated with light. Thus, the high antibacterial efficacy of their flexible film primarily came from PFEMO's interaction with light, rather than a simple interaction between the nanoparticles and the substrate. Due to this, the morphological controllability

of the nanoparticle formation on the surface was not extensively discussed. Although the antibacterial efficiency of the flexible film was favorable, the synthesis was more complicated than our nanoplatelet synthesis, and it also involved the addition of metal ions to a polymer surface rather than using ions directly from a metal surface.

Gunell et al. developed another example of a nanoparticle-coated surface with antibacterial properties by using direct and indirect liquid flame spray to form silver nanoparticle coatings on glass, polyethylene, and polyethylene terephthalate surfaces.[78] They used a precursor solution composed of silver nitrate in deionized water, forming particles by injecting the precursor solution in turbulent $H_2/O_2/N_2$ flame. Nanoparticles were deposited on the surfaces directly by passing the samples through the flame, or indirectly after passing the flame through a flow tube. The antibacterial efficacy was evaluated for surfaces with different numbers of coating layers, as well as for multiple strains of bacteria. To do this, bacterial suspensions were dropped onto the nanoparticle-coated samples and incubated for 6 to 48 h. The samples were then stamped on top of blood agar plates to transfer viable bacteria from the samples to the agar surfaces. Samples were then incubated and the number of CFUs was counted the following day. They found that the number of coating cycles, the surface that was coated, and the type of bacteria, each had an effect on the antibacterial efficacy of the coated surfaces. At least 30 coating cycles were needed to inhibit the growth of *S. aureus* on PE and PET samples. On the other hand, a single coating cycle was enough to give glass antibacterial properties against *E. coli*. They also found that direct deposition of the particles led to better antibacterial efficacy than indirect deposition. In terms of synthetic complexity, the preparation of their precursor is comparable in simplicity to the preparation of the nanoplatelet precursor solution in our work. However, the liquid flame spray synthesis process does require some specialized equipment. Despite this, the use of the liquid flame spray synthesis process provides the advantage of controlling the distribution and number of particles on the surface based on the number of coating cycles applied to the sample. Further studies would need to be conducted on the nanoplatelets to determine which synthesis parameters can be adjusted to achieve greater control over their size and distribution.

Li et al. generated copper nanoparticles in situ in flexible polyurethane foams by placing the foams in copper sulfate solutions at 80 °C.[79] This led to the hydrothermal formation of copper nanoparticles, in the size range of approximately 100 to 130 nm, that was generated on the surface of cell walls within the polyurethane foams. They observed increased tensile and compressive strength in the polyurethane foams as a result of the copper nanoparticle incorporation into the foam structure. Finally, they tested the antibacterial properties of 10 mm discs of polyurethane foams which contained copper nanoparticles that had been incorporated into the structures by reaction with different concentrations of copper sulfate solutions. After 48 h of incubation, they observed good antibacterial activity against *E. coli*, *Pseudomonas aeruginosa*, *S. aureus*, and *Bacillus licheniformis*, with an inhibition zone of up to 40 mm in some cases. The synthetic simplicity of this method is apparent. However, the use of a hydrothermal synthesis method to form the nanoparticles makes the synthesis more involved than our room-temperature single-step synthesis of the copper nanoplatelets. Despite this, their method of synthesis enabled excellent control over the copper nanoparticle size simply by changing the concentration of copper sulfate used.

Overall, in situ synthesis of antibacterial nanoparticles on surfaces is of great interest and a field that is continuing to grow. Various approaches and materials can be used to achieve these antibacterial properties, and each approach carries its own strengths and weaknesses. The strength of our method lies in its synthetic simplicity compared to other methods, and can potentially be used to improve the antibacterial properties of a wide range of copper surfaces.

## 3. Conclusion

We have developed a simple method to assemble metal-based nanostructures directly on metal surfaces without the need for the prior synthesis of nanoparticles or the inclusion of any metals within the precursor solution. We demonstrated that nanoplatelets could be formed on a variety of copper surfaces and explored their potential for use in antibacterial surfaces. We found that the copper surfaces with nanoplatelets had improved antibacterial activity compared to copper surfaces without nanoplatelets, likely as a result of an increased surface area from which copper ions can dissolve. Antibacterial activity was demonstrated against *E. coli*, MDR *E. coli*, MDR *S. aureus*, MDR *A. baumannii*, and *S. mutans*. Copper surfaces covered with nanoplatelets also induced structural and morphological changes in bacterial cells and led to changes in protein and DNA expression. We further demonstrated that the expression of specific proteins related to cell division, copper toxicity, and DNA division were altered as a result of the presence of nanoplatelets. Lastly, we demonstrated that other nanostructures could be formed by depositing our simple aqueous diluted HCl solution onto various metal surfaces. Overall, this study provides a simple method by which metal-based surfaces, especially those containing copper, can be modified to incorporate 2D nanostructures.

## 4. Experimental Section

*Materials*: Copper granules, zinc strips, tin chips, and cobalt pieces were purchased from Chemistry Cabinet.[80] Other metal samples were obtained in the form of a copper anode sheet and zinc anode sheet. 300 to 400 mesh carbon-coated copper TEM grids were purchased from Ted Pella.[80] Regular *E. coli*, multi-drug-resistant *E. coli* (ATCC BAA-201), multidrug-resistant *A. baumannii* (ATCC BAA-1605), and multidrug-resistant *S. aureus* (ATCC BAA-38) were purchased from ATCC.[80] Loctite Clear Silicone Waterproof Sealant[80] was used to adhere copper substrate samples to the wells of 24-well plates. DNA extraction was conducted using a ZymoBIOMICS DNA Miniprep Kit (Zymo Research).[80] Protein extraction was conducted using a Qproteome Bacterial Protein Prep Kit (Qiagen),[80] and protein digestions were conducted using an In-Solution Tryptic Digestion and Guanidination Kit (89 895, ThermoFisher Scientific).[80] CM-$H_2$DCFDA and the LIVE/DEAD BacLight Bacterial Viability Kit were purchased as kits from ThermoFisher Scientific.[80] The Cell Meter TUNEL apoptosis assay kit was purchased from AAT Bioquest.[80]

*Preparation of Nanoplatelet Precursor Solution*: *Solution for Cu@HCl NP*: 50 µL of 2N HCl was diluted with 1 mL of filtered water.

*Solution for Cu@HCl-$NH_2$ NP*: 3.5 µL 2 2′-(ethylenedioxy) bis(ethylamine) was diluted in 10 mL of filtered water. 50 µL of 2N HCl was added to 1 mL of this solution.

*Synthesis of Nanoplatelets*: *On TEM Grids*: 2.5 µL of precursor solution was drop-cast onto the uncoated side of carbon-coated copper TEM grids. Samples were allowed to dry for 2 min, after which excess liquid was removed using filter paper. The TEM grid was then allowed to dry until the imaging was conducted.

*On Copper Tape and Other Metal Substrates*: 3.5 µL of precursor solution was drop-cast onto the substrate and allowed to completely dry under atmospheric conditions. For bacterial experiments, eight 3.5 µL drops of precursor solution were deposited on each 2 cm copper sample.

*Varying Synthesis Parameters*: Syntheses were repeated on copper tape as described above but with varying the ratio of diamine to HCl in the precursor solution, as well as preparing different dilutions of the precursor solution prior to dropping it on the copper tape. Details of each concentration tested are provided in Figure 3D.

*Scanning Electron Microscopy of Nanoplatelet Samples*: Samples were imaged using a commercial environmental SEM at nominal acceleration voltages of 10 to 20 kV. Samples were not coated prior to imaging.

*FT-IR and XRD*: FT-IR samples were prepared by adhering copper tape samples directly onto corner frosted FT-IR slides. FT-IR measurements were taken with a commercial FT-IR spectrometer. XRD was conducted on powder samples using a commercial XRD system. XRD spectra were collected for nanoplatelet samples directly on the Cu tape substrate.

*Bacterial Culture*: *A. baumannii* (ATCC BAA-1605), and multidrug-resistant *S. aureus* (ATCC BAA-38) were cultured at 37 °C under aerobic conditions in Tryptic Soy broth overnight with shaking at 200 rpm. *E. coli* was cultured in Luria-Bertani (LB) broth at 37 °C under aerobic conditions. MDR *E. coli* was cultured at 37 °C under aerobic conditions in Tryptic Soy Medium supplemented with 10 µg $mL^{-1}$ Ceftazidime. *S. mutans* was cultured in brain heart infusion (BHI) broth.

*Bacterial Optical Density Experiments*: Copper substrates or nanoplatelet samples were adhered to the wells of a 24-well plate using waterproof silicone glue. Two 2 cm sample strips were used for each well. The glue was allowed to completely dry before experiments were conducted. 2 mL of bacteria with an optical density of approximately 0.25 were added to each well of the 24-well plates. OD600 values were measured kinetically at 37 °C for 4 h in a plate reader. Fold change was calculated by dividing the background-subtracted OD600 value at 4 h by the background-subtracted initial OD600 value, where a fold change of 1 would indicate no change in OD600 value between the initial and final measurement. For *S. mutans*, the OD600 values were initially measured for 2 hours, after which the OD600 values were measured for another 2 h beginning at the 2.5 h mark. This was due to the initial setup of the plate reader software which was only collecting 2 h of data at a time.

*E. coli 24 h Optical Density Experiments*: Bacterial optical density experiments were repeated for *E. coli* following the method above, but with measurements taken every 20 min for 24 h.

*Bacterial Optical Density Experiments Using Precursor Solutions*: 2 mL of MDR *E. coli* bacteria with an optical density of approximately 0.25 was added to 12 wells of a 24-well plate. 2 mL of bacterial broth were added to the remaining 12 wells of a 24-well plate. For treatment groups, 56 µL of nanoplatelet precursor solution was added to each well. OD600 values were measured kinetically at 37 °C for 4 h in a plate reader.

*Scanning Electron Microscopy of Substrates Used to Treat Bacteria*: 2 mL of MDR *E. coli* with an initial optical density of approximately 0.25 was exposed to two 2 cm long copper tape samples or nanoplatelet samples for 4 h at 37 °C in an incubator-shaker. Following this, samples were fixed in a 2% paraformaldehyde, 2.5% glutaraldehyde solution for 10 min, and sequentially dehydrated in solutions of 25%, 50%, 75%, 95%, and 100% ethanol for 10 min each. The samples were then allowed to dry under atmospheric conditions. Prior to imaging, samples were coated with platinum-palladium. Samples were imaged on a commercial SEM with a 10 kV nominal acceleration voltage.

*Scanning Electron Microscopy of Bacteria after Exposure to Substrates*: 2 mL of MDR *E. coli* with an initial optical density of approximately 0.25 was exposed to two 2 cm long copper tape samples or nanoplatelet samples for 4 h at 37 °C in an incubator shaker. Following this, the bacterial suspensions were centrifuged at 626 rad $s^{-1}$ (5976 rpm), 39 200 m $s^{-2}$ (4000 × *g*) for 15 min, and resuspended in 0.5 mL 2% volume fraction paraformaldehyde/water solution, 2.5% volume fraction glutaraldehyde/water solution for 10 min. The suspensions were then centrifuged for 10 min and resuspended in 25% volume fraction ethanol/water solution for 10 min. Suspensions were then sequentially centrifuged (626 rad $s^{-1}$ (5976 rpm), 39 200 m $s^{-2}$ (4000 × *g*), 5 min) and resuspended in 0.5 mL of 50%, 75%, and 95% volume fraction ethanol/water solutions, with samples retained in each solution for 5 min prior to centrifugation. Finally, the samples were in 250 µL 100% ethanol, and 50 µL of each sample was deposited onto a glass coverslip and allowed to dry under atmospheric conditions. Prior to imaging, samples were coated with platinum-palladium. Samples were imaged on a commercial SEM with a 10 kV nominal acceleration voltage.

*Bacterial Agar Colony Growth Inhibition Studies*: Pre-poured LB agar plates with 100 µg $mL^{-1}$ ampicillin were used for this experiment. 100 µL of ampicillin-resistant *E. coli* with OD600 = 0.6 was added to the surface of the agar plate and spread equally. Next, the nanoplatelet samples were placed face-down on the surface of the LB agar and then incubated at 37 °C for 24 h.

*ROS Generation Assay*: 50 µg CM-$H_2$DCFDA dye was dissolved in 8.65 µL dimethyl sulfoxide [DMSO], and 8 µL of this solution was added to 8 mL bacterial broth. 20 mL of bacteria was suspended at an OD600 value of 0.25. The bacteria were centrifuged at 700 rad $s^{-1}$ (6682 rpm), 49 000 m $s^{-2}$ (5000 × *g*) for 5 min and then resuspended in the bacterial medium containing the CM-$H_2$DCFDA dye. The bacteria were protected from light and incubated in a shaker incubator at 37 °C for 5 min. The suspension was then centrifuged at 626 rad $s^{-1}$ (5976 rpm), 39 200 m $s^{-2}$ (4000 × *g*) for 5 min, and the bacteria was resuspended in 8 mL fresh medium. The centrifugation process was repeated one more time, and the bacterial pellet was finally resuspended in 20 mL fresh medium. 1 mL of bacterial suspension was placed in each centrifuge tube, and the suspensions were treated with the copper tape or nanoplatelets, after which fluorescence measurements were collected in accordance with kit directions.

*Live-Dead Assay*: 2 mL of MDR *E. coli* with an initial optical density of approximately 0.25 was exposed to two 2 cm long copper tape samples or nanoplatelet samples for 4 h at 37 °C in an incubator shaker. Following this, 0.75 mL of each sample was collected and centrifuged to form a bacterial cell pellet. The pellet was then resuspended in NaCl solution with a volume fraction of 0.85%, and three 100 µL aliquots from each solution were added into the wells of a 96-well plate. 100 µL of live-dead solution (prepared according to manufacturer guidelines) was added to each well. Samples were incubated in the dark at room temperature for 15 min, after which fluorescence spectra were collected

*TUNEL Assay*: 2 mL of MDR *E. coli* with an initial optical density of approximately 0.25 was exposed to two 2 cm long copper tape samples or nanoplatelet samples for 4 h at 37 °C in an incubator-shaker. Following this, 0.75 mL of each sample was collected and centrifuged to form a bacterial cell pellet. Each pellet was then resuspended in 150 µL TUNEL solution (12.5 µL tunnelyte diluted in 1.25 mL reaction buffer) and placed on an incubator-shaker at 37 °C for 1 h. Samples were then pelleted and resuspended in 300 µL reaction buffer and three 100 µL aliquots (3 technical replicates) of each sample were pipetted into the wells of a 96-well plate. Fluorescence spectra were collected for each well (excitation 550 nm, emission range: 590 nm to 650 nm, gain of 150), and the peak emission intensity was averaged across all technical replicates for each sample.

*DNA Extraction*: 2 mL of MDR *E. coli* with an initial optical density of approximately 0.25 was exposed to two 2 cm long copper tape samples or nanoplatelet samples for 4 h at 37 °C in an incubator shaker. DNA was extracted following the guidelines provided by the kit manufacturer. Samples were stored frozen at -20 °C until further use.

*DNA Gel Electrophoresis*: Agarose gels were prepared by adding 2 g agarose to 100 mL Tris-Borate-EDTA (TBE) buffer and heating the solution in a microwave. Ethidium bromide was added into the solution, and the gel was poured into the mold and allowed to cool. 50 ng of each DNA sample was added to their respective wells, and the gel was run at 120 V for 75 min.

*Protein Extraction*: 2 mL of MDR *E. coli* with an initial optical density of approximately 0.25 was exposed to two 2 cm long copper tape samples or nanoplatelet samples for 4 h at 37 °C in an incubator-shaker. Water-soluble

proteins were then extracted from bacteria following the guidelines in the obtained kit. Samples were stored frozen at -80 °C until further use.

*SDS PAGE*: Protein concentration was determined and samples were diluted to a concentration of 1 μg $\mu L^{-1}$ and run on a 7.5% precast gel at 115 V for 48 min, after which they were stained and imaged on a gel imager.

*Statistical Analysis*: Statistical analysis was conducted with two-tailed Student's T-tests. Bonferroni corrections were used to determine adjusted *P* values in cases where multiple comparisons were conducted.

*Proteomics Analysis*: Protein concentration was determined using a Nanodrop.[80] Samples were diluted to a concentration of 1 μg $\mu L^{-1}$ and a 10 μL aliquot was digested following the kit instructions. Samples were stored at -20 °C and submitted to the UMBC Molecular Characterization and Analysis Complex for label-free proteomic analysis.

## Supporting Information

Supporting Information is available from the Wiley Online Library or from the author.

## Acknowledgements

The authors gratefully acknowledge Dr. Priyanka Ray for her helpful comments and assistance with electrophoresis experiments, as well as Dr. Aaron Schwartz-Duval for his helpful comments. This project was partially funded through grants from the National Institutes of Health, Department of Defense, and University of Illinois. P.F. was supported by the National Physical Science Consortium and the National Institute of Standards & Technology through a National Physical Science Consortium (NPSC) graduate fellowship and by the Nadine Barrie Smith Memorial Fellowship from the Beckman Institute. Research reported in this publication was supported by the National Institute of Biomedical Imaging and Bioengineering of the National Institutes of Health under Award Number T32EB019944. This work was carried out in part in the Frederick Seitz Materials Research Laboratory Central Research Facilities, University of Illinois. Figure 1 was created using BioRender (www.biorender.com).

## Conflict of Interest

Prof. Pan is the founder or co-founder of three University-based start ups. None of these entities, however, supported this work.

## Data Availability Statement

The data that support the findings of this study are available from the corresponding author upon reasonable request.

## Keywords

2D, antibacterials, coating, nanoparticles, nanoplatelets, surface modification

[1] L. Cobrado, A. Silva-Dias, M. M. Azevedo, A. G. Rodrigues, *Eur. J. Clin. Microbiol. Infect. Dis.* **2017**, *36*, 2053.
[2] L. Hall-Stoodley, J. W. Costerton, P. Stoodley, *Nat. Rev. Microbiol.* **2004**, *2*, 95.
[3] N. Høiby, T. Bjarnsholt, M. Givskov, S. Molin, O. Ciofu, *Int. J. Antimicrob. Agents* **2010**, *35*, 322.
[4] M. Kostakioti, M. Hadjifrangiskou, S. J. Hultgren, *Cold Spring Harbor Perspect. Med.* **2013**, *3*, a010306.
[5] S. Singh, S. K. Singh, I. Chowdhury, R. Singh, *Open Microbiol. J.* **2017**, *11*, 53.
[6] S. Divakar, M. Lama, K. U. Asad, *Antimicrob. Resist. Infect. Control* **2019**, *8*, 76.
[7] X. M. Yang, J. W. Hou, Y. Tian, J. Y. Zhao, Q. Q. Sun, S. B. Zhou, *Sci. China: Technol. Sci.* **2022**, *65*, 1000.
[8] A. P. Ramos, M. A. E. Cruz, C. B. Tovani, P. Ciancaglini, *Biophys. Rev.* **2017**, *9*, 79.
[9] S. K. Murthy, *Int. J. Nanomed.* **2007**, *2*, 129.
[10] P. Fathi, J. S. Khamo, X. Huang, I. Srivastava, M. B. Esch, K. Zhang, D. Pan, *Carbon* **2019**, *145*, 572.
[11] P. Fathi, D. Pan, *Nanomedicine* **2020**, *15*, 2493.
[12] N. Zahin, R. Anwar, D. Tewari, M. T. Kabir, A. Sajid, B. Mathew, M. S. Uddin, L. Aleya, M. M. Abdel-Daim, *Environ. Sci. Pollut. Res.* **2020**, *27*, 19151.
[13] A. K. Pearce, T. R. Wilks, M. C. Arno, R. K. O. Reilly, *Nat. Rev. Chem.* **2021**, *5*, 21.
[14] Z. Zhao, A. Ukidve, V. Krishnan, A. Fehnel, D. C. Pan, Y. Gao, J. Kim, M. A. Evans, A. Mandal, J. Guo, V. R. Muzykantov, S. Mitragotri, *Nat. Biomed. Eng.* **2021**, *5*, 441.
[15] N. N. Parayath, S. B. Stephan, A. L. Koehne, P. S. Nelson, M. T. Stephan, *Nat. Commun.* **2020**, *11*, 6080.
[16] S. Liu, X. Chen, L. Bao, T. Liu, P. Yuan, X. Yang, X. Qiu, J. J. Gooding, Y. Bai, J. Xiao, F. Pu, Y. Jin, *Nat. Biomed. Eng.* **2020**, *4*, 1063.
[17] F. Benfenati, G. Lanzani, *Nat. Rev. Mater.* **2021**, *6*, 1.
[18] J. G. Croissant, K. S. Butler, J. I. Zink, C. J. Brinker, *Nat. Rev. Mater.* **2020**, *5*, 886.
[19] P. Fathi, H. J. Knox, D. Sar, I. Tripathi, F. Ostadhossein, S. K. Misra, M. B. Esch, J. Chan, D. Pan, *ACS Nano* **2019**, *13*, 7690.
[20] L. Mao, L. Wang, M. Zhang, M. W. Ullah, L. Liu, W. Zhao, Y. Li, A. A. Q. Ahmed, H. Cheng, Z. Shi, G. Yang, *Adv. Healthcare Mater.* **2021**, *10*, 2100402.
[21] T. Ma, X. Zhai, Y. Huang, M. Zhang, X. Zhao, Y. Du, C. Yan, *Adv. Healthcare Mater.* **2021**, *10*, 2100033.
[22] M. Alafeef, K. Dighe, D. Pan, *ACS Appl. Mater. Interfaces* **2019**, *11*, 42943.
[23] M. Alafeef, P. Moitra, D. Pan, *Biosens. Bioelectron.* **2020**, *165*, 112276.
[24] Y. Wang, Y. Yang, Y. Shi, H. Song, C. Yu, *Adv. Mater.* **2020**, *32*, 1904106.
[25] D. P. Linklater, V. A. Baulin, X. L. Guével, J. B. Fleury, E. Hanssen, T. H. P. Nguyen, S. Juodkazis, G. Bryant, R. J. Crawford, P. Stoodley, E. P. Ivanova, *Adv. Mater.* **2020**, *32*, 2005679.
[26] G. Wang, K. Tang, Z. Meng, P. Liu, S. Mo, B. Mehrjou, H. Wang, X. Liu, Z. Wu, P. K. Chu, *Adv. Mater.* **2020**, *32*, 2003616.
[27] M. Ye, Y. Zhao, Y. Wang, M. Zhao, N. Yodsanit, R. Xie, D. Andes, S. Gong, *Adv. Mater.* **2021**, *33*, 2006772.
[28] X. Xie, T. C. Sun, J. Xue, Z. Miao, X. Yan, W. W. Fang, Q. Li, R. Tang, Y. Lu, L. Tang, Z. Zha, T. He, *Adv. Funct. Mater.* **2020**, *30*, 2000511.
[29] A. Ivanova, K. Ivanova, A. Tied, T. Heinze, T. Tzanov, *Adv. Funct. Mater.* **2020**, *30*, 2001284.
[30] P. Makvandi, C. Yu Wang, E. N. Zare, A. Borzacchiello, L. na Niu, F. R. Tay, *Adv. Funct. Mater.* **2020**, *30*, 1910021.
[31] G. Mi, D. Shi, M. Wang, T. J. Webster, *Adv. Healthcare Mater.* **2018**, *7*, 1800103.
[32] T. Dai, B. Guo, G. Qi, S. Xu, C. Zhou, G. C. Bazan, B. Liu, *Adv. Healthcare Mater.* **2021**, *10*, 2100885.
[33] R. Agarwal, C. T. Johnson, B. R. Imhoff, R. M. Donlan, N. A. McCarty, A. J. García, *Nat. Biomed. Eng.* **2018**, *2*, 841.
[34] S. Hussain, J. Joo, J. Kang, B. Kim, G. B. Braun, Z. G. She, D. Kim, A. P. Mann, T. Mölder, T. Teesalu, S. Carnazza, S. Guglielmino, M. J. Sailor, E. Ruoslahti, *Nat. Biomed. Eng.* **2018**, *2*, 95.

[35] J. Lee, J. Yoo, J. Kim, Y. Jang, K. Shin, E. Ha, S. Ryu, B. G. Kim, S. Wooh, K. Char, *ACS Appl. Mater. Interfaces* **2019**, *11*, 6550.
[36] S. A. Jalil, M. Akram, J. A. Bhat, J. J. Hayes, S. C. Singh, M. ElKabbash, C. Guo, *Appl. Surf. Sci.* **2020**, *506*, 144952.
[37] Y. Wang, T. Wei, Y. Qu, Y. Zhou, Y. Zheng, C. Huang, Y. Zhang, Q. Yu, H. Chen, *ACS Appl. Mater. Interfaces* **2020**, *12*, 21283.
[38] F. A. Bezza, S. M. Tichapondwa, E. M. N. Chirwa, *Sci. Rep.* **2020**, *10*, 16680.
[39] S. Tang, J. Zheng, *Adv. Healthcare Mater.* **2018**, *7*, 201701503.
[40] R. Bai, L. Peng, Q. Sun, Y. Zhang, L. Zhang, Y. Wei, B. Han, *Materials* **2020**, *13*, 4594.
[41] A. Elbourne, S. Cheeseman, P. Atkin, N. P. Truong, N. Syed, A. Zavabeti, M. Mohiuddin, D. Esrafilzadeh, D. Cozzolino, C. F. McConville, M. D. Dickey, R. J. Crawford, K. Kalantar-Zadeh, J. Chapman, T. Daeneke, V. K. Truong, *ACS Nano* **2020**, *14*, 802.
[42] L. Ye, Z. Cao, X. Liu, Z. Cui, Z. Li, Y. Liang, S. Zhu, S. Wu, *J. Alloys Compd.* **2022**, *904*, 164091.
[43] V. T. Nguyen, K. S. Trinh, *Braz. J. Chem. Eng.* **2019**, *36*, 1553.
[44] A. C. Pinho, A. P. Piedade, *Polymers* **2020**, *12*, 2469.
[45] Z. Wang, L. Mei, X. Liu, Q. Zhou, *Colloids Surf., B* **2021**, *204*, 111802.
[46] Y. Xiang, J. Li, X. Liu, Z. Cui, X. Yang, K. W. K. Yeung, H. Pan, S. Wu, *Mater. Sci. Eng. C* **2017**, *79*, 629.
[47] Y. Q. Zhao, Y. Sun, Y. Zhang, X. Ding, N. Zhao, B. Yu, H. Zhao, S. Duan, F. J. Xu, *ACS Nano* **2020**, *14*, 2265.
[48] G. Mi, D. Shi, M. Wang, T. J. Webster, *Adv. Healthcare Mater.* **2018**, *7*, e1800103.
[49] C. Zwahr, R. Helbig, C. Werner, A. F. Lasagni, *Sci. Rep.* **2019**, *9*, 6721.
[50] J. Rosenbaum, D. L. Versace, S. Abbad-Andallousi, R. Pires, C. Azevedo, P. Cénédese, P. Dubot, *Biomater. Sci.* **2017**, *5*, 455.
[51] R. Liu, Y. Tang, L. Zeng, Y. Zhao, Z. Ma, Z. Sun, L. Xiang, L. Ren, K. Yang, *Dent. Mater.* **2018**, *34*, 1112.
[52] S. Mittapally, R. Taranum, S. Parveen, *J. Drug Delivery Ther.* **2018**, *8*, 411.
[53] P. Singha, J. Locklin, H. Handa, A. B. Author, *Acta Biomater.* **2017**, *50*, 20.
[54] R. Liu, K. Memarzadeh, B. Chang, Y. Zhang, Z. Ma, R. P. Allaker, L. Ren, K. Yang, *Sci. Rep.* **2016**, *6*, 29985.
[55] M. Astasov-Frauenhoffer, S. Koegel, T. Waltimo, A. Zimmermann, C. Walker, I. Hauser-Gerspach, C. Jung, *J. Mater. Sci.: Mater. Med.* **2019**, *30*, 84.
[56] D. Mitra, E. T. Kang, K. G. Neoh, *ACS Appl. Mater. Interfaces* **2020**, *12*, 21159.
[57] M. L. Ermini, V. Voliani, *ACS Nano* **2021**, *15*, 6008.
[58] C. Ching, M. H. Zaman, *Sci. Rep.* **2020**, *10*, 8754.
[59] S. Mukherjee, R. E. Mosci, C. M. Anderson, B. A. Snyder, J. Collins, J. T. Rudrik, S. D. Manning, **2017**, *23*, 1609.
[60] B. Ghanem, R. N. Haddadin, *Antimicrob. Resist. Infect. Control* **2018**, *7*, 47.
[61] S. K. Miryala, S. Ramaiah, *Genomics* **2019**, *111*, 958.
[62] D. A. Tadesse, S. Zhao, E. Tong, S. Ayers, A. Singh, M. J. Bartholomew, P. F. McDermott, *Emerging Infect. Dis.* **2012**, *18*, 741.
[63] Antibiotic Resistance Threats in the United States, Atlanta, GA **2019**. https://www.cdc.gov/drugresistance/pdf/threats-report/2019-ar-threats-report-508.pdf (accessed: July 2022)
[64] R. S. Oguike, O. Oni, A. U. Barambu, D. Balarak, T. Buba, C. U. Okeke, L. S. Momoh, S. Onimisi, W. J. Nwada, *Comput. Chem.* **2021**, *09*, 18.
[65] S. El Issami, L. Bazzi, M. Mihit, B. Hammouti, S. Kertit, E. A. Addi, R. Salghi, *Pigm. Resin Technol.* **2007**, *36*, 161.
[66] Sudheer, M. A. Quraishi, *Corros. Sci.* **2013**, *70*, 161.
[67] M. A. Deyab, *J. Ind. Eng. Chem.* **2015**, *22*, 384.
[68] A. Giachino, K. J. Waldron, *Mol. Microbiol.* **2020**, *114*, 377.
[69] H. J. Park, T. T. M. Nguyen, J. Yoon, C. Lee, *Environ. Sci. Technol.* **2012**, *46*, 11299.
[70] Y. Wang, J. Ma, Q. Xu, J. Zhang, *Mater. Des.* **2017**, *113*, 240.
[71] S. Mathews, M. Hans, F. Mücklich, M. Solioz, *Appl. Environ. Microbiol.* **2013**, *79*, 2605.
[72] E. J. Nkuwi, F. Kabanangi, A. Joachim, S. Rugarabamu, M. Majigo, *BMC Res. Notes* **2018**, *11*, 4.
[73] T. Sexton, P. Clarke, E. O'Neill, T. Dillane, H. Humphreys, *J. Hosp. Infect.* **2006**, *62*, 187.
[74] A. Rózańska, A. Chmielarczyk, D. Romaniszyn, G. Majka, M. Bulanda, *Antimicrob. Resist. Infect. Control* **2018**, *7*, 10.
[75] J. A. Lemos, S. R. Palmer, L. Zeng, Z. T. Wen, J. K. Kajfasz, I. A. Freires, J. Abranches, L. J. Brady, *Microbiol. Spectrum* **2019**, *7*, https://doi.org/10.1128/microbiolspec.GPP3-0051-2018
[76] M. Yasuyuki, K. Kunihiro, S. Kurissery, N. Kanavillil, Y. Sato, Y. Kikuchi, *Biofouling* **2010**, 851.
[77] X. Wang, S. Zhu, L. Liu, L. Li, *ACS Appl. Mater. Interfaces* **2017**, *9*, 9051.
[78] M. Gunell, J. Haapanen, K. J. Brobbey, J. J. Saarinen, M. Toivakka, J. M. Mäkelä, P. Huovinen, E. Eerola, *Nanotechnol. Sci. Appl.* **2017**, *10*, 137.
[79] C. Li, H. Ye, S. Ge, Y. Yao, B. Ashok, N. Hariram, H. Liu, H. Tian, Y. He, G. Guo, A. V. Rajulu, *J. Mater. Res. Technol.* **2022**, *19*, 3603.
[80] Commercial entities, equipment, or materials may be identified in this document to describe an experimental procedure or concept adequately. Such identification is not intended to imply recommendation or endorsement by the National Institute of Standards and Technology, nor is it intended to imply that the entities, materials, or equipment are necessarily the best available for the purpose.